HAARP DIAGNOSTIC INSTRUMENTS; HIGH FREQUENCY ACTIVE AURORAL RESEARCH PROGRAM

Paul A. Kossey
James C. Battis
Editors

December 2002

AIR FORCE RESEARCH LABORATORY
Space Vehicles Directorate
29 Randolph Road
AIR FORCE MATERIEL COMMAND
HANSCOM AFB, MA 01731-3010

AFRL-VS-TR-2003-1570

This report has been approved for publication.

____//signed//_____
PAUL A. KOSSEY
Project Manager

FOR THE COMMANDER

____//signed//_____
WILLIAM F. DENIG
Chief, Space Weather COE

____//signed//_____
JOHN B. WISSLER, Lt Col, USAF
Chief, Battlespace Environment Division

REPORT DOCUMENTATION PAGE

Public reporting burden for this collection of information is estimated to average 1 hour per response, including the time for reviewing instructions, searching existing data sources, gathering and maintaining the data needed, and completing and reviewing this collection of information. Send comments regarding this burden estimate or any other aspect of this collection of information, including suggestions for reducing this burden to Department of Defense, Washington Headquarters Services, Directorate for Information Operations and Reports (0704-0188), 1215 Jefferson Davis Highway, Suite 1204, Arlington, VA 22202-4302. Respondents should be aware that notwithstanding any other provision of law, no person shall be subject to any penalty for failing to comply with a collection of information if it does not display a currently valid OMB control number. **PLEASE DO NOT RETURN YOUR FORM TO THE ABOVE ADDRESS.**

1. REPORT DATE (DD-MM-YYYY)	2. REPORT TYPE	3. DATES COVERED (From - To)
09-06-03	Interim Scientific	01 Oct 2002 to 30 Sep 2003

4. TITLE AND SUBTITLE
HAARP Diagnostic Instruments; High Frequency Active Auroral Research Program

5a. CONTRACT NUMBER

5b. GRANT NUMBER

5c. PROGRAM ELEMENT NUMBER
62601F

6. AUTHOR(S)
Paul A. Kossey and James C. Battis, Editors

5d. PROJECT NUMBER
4827

5e. TASK NUMBER
HA

5f. WORK UNIT NUMBER
R1

7. PERFORMING ORGANIZATION NAME(S) AND ADDRESS(ES)

Air Force Research Laboratory
29 Randolph Road
Hanscom Air Force Base, MA 01731-3010

8. PERFORMING ORGANIZATION REPORT NUMBER

AFRL-VS-TR-2003-1570

9. SPONSORING / MONITORING AGENCY NAME(S) AND ADDRESS(ES)
Air Force Research Laboratory
29 Randolph Road
Hanscom Air Force Base, MA 01731-3010

10. SPONSOR/MONITOR'S ACRONYM(S)

11. SPONSOR/MONITOR'S REPORT NUMBER(S)
AFRL-VS-TR-2003-1570

12. DISTRIBUTION / AVAILABILITY STATEMENT
Approved for public release; distribution unlimited

20040914 026

13. SUPPLEMENTARY NOTES

14. ABSTRACT This report describes the suite of diagnostic instruments at a major facility for experimental radio science research, under development in Gakona, Alaska. This site is being developed as part of the High Frequency Active Auroral Research Program (HAARP). A key objective of the program is the identification and characterization of the physical processes initiated in the ionosphere and space via interactions with high power radio waves. Among these phenomena are: plasma instabilities and turbulence; electron acceleration, including the production of optical and infrared (IR) emissions; the generation, maintenance and/or suppression of ionization structures aligned along the earth's magnetic field; the modulation of currents in the ionosphere, thereby producing virtual antennas in space to generate ULF/ELF/VLF radio waves; and the production of stimulated electromagnetic emissions (SEE). The efficiencies that can be obtained in the initiation, maintenance, and control of such processes and techniques to excite selected (individual) processes, or to suppress unwanted ones, are also research areas of increasing interest. To provide the experimental capabilities required to meet its objectives, the HAARP Gakona facility includes a powerful, phased-array, high-frequency (HF) transmitter and an extensive complement of radio-frequency and optical diagnostic instruments.

15. SUBJECT TERMS HAARP, Ionospheric Physics, Ionosphere, Radio Science, Ionosonde, Riometer, Magnetometer, Backscatter Radar, ELF/VLF Receiver, ELF/VLF Radiometer, TEC, Scintillation, Optical Imaging, UHF Radar

16. SECURITY CLASSIFICATION OF:			17. LIMITATION OF ABSTRACT	18. NUMBER OF PAGES	19a. NAME OF RESPONSIBLE PERSON Paul A. Kossey
a. REPORT	**b. ABSTRACT**	**c. THIS PAGE**			**19b. TELEPHONE NUMBER** (include area code) 781-377-4669
Unclassified	Unclassified	Unclassified	SAR		

Contents

Acknowledgements

HAARP Diagnostic Instruments

1. Introduction
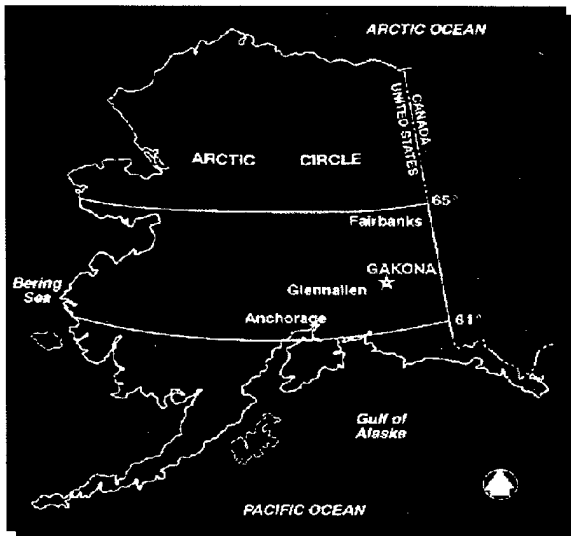
Figure 1. Location of the HAARP research facility.

This report describes diagnostic instruments at a major facility for experimental radio science research, under development in Gakona, Alaska (Figure 1, Figure 2), as part of the High Frequency Active Auroral Research Program (HAARP). The program is jointly managed by the Air Force Research Laboratory and the Office of Naval Research. A key objective of the program is the identification and characterization of the physical processes initiated in the ionosphere and space by interactions with high power radio waves. Among these are: plasma instabilities and turbulence; electron

Figure 2. Aerial view of the research facility under development in Gakona, Alaska.

1

acceleration, including the production of optical and infrared (IR) emissions; the generation, maintenance and/or suppression of ionization structures aligned along the earth's magnetic field; the modulation of currents in the ionosphere, thereby producing virtual antennas in space to generate ULF/ELF/VLF radio waves; and the production of stimulated electromagnetic emissions (SEE). The efficiencies that can be obtained in the initiation, maintenance, and control of such processes and techniques to excite selected (individual) processes, or to suppress unwanted ones, are also research areas of increasing interest. Other program objectives include experimental research to assess the potential for exploiting this emerging ionosphere technology for new radio wave system applications, and the use of the facility to support collaborative research programs such as those associated with global change and the National Science Foundation's Space Weather Initiative. To provide the experimental capabilities required to meet its objectives, the HAARP Gakona facility includes a powerful, phased-array, high-frequency (HF) transmitter and an extensive complement of radio-frequency and optical diagnostic instruments (Figure 3).

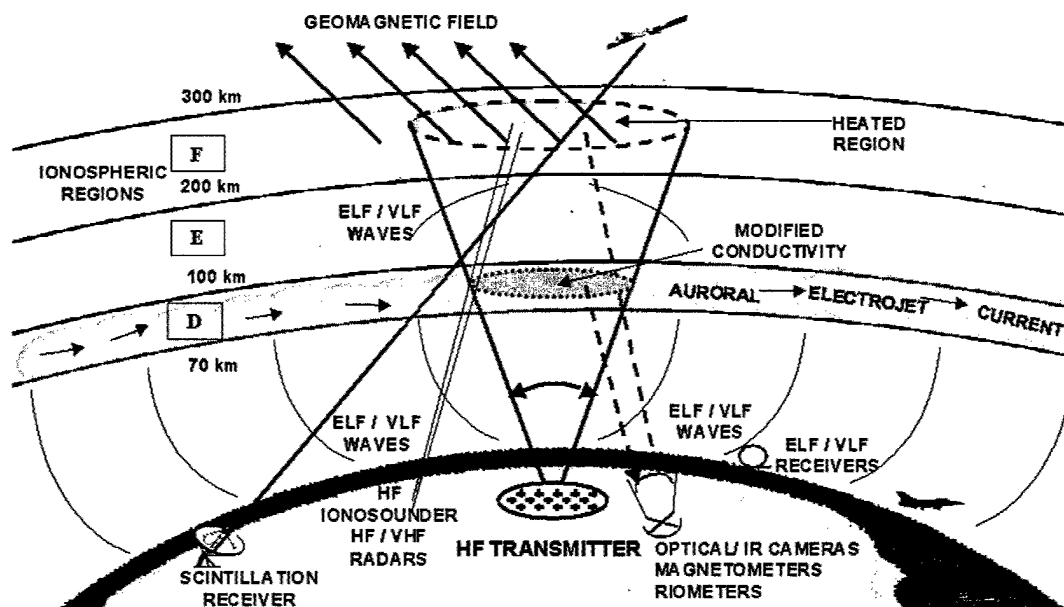
Figure 3. Notional picture of the HAARP facility with its HF transmitter and suite of diagnostic instruments.

2. HF Transmitter

Currently, the HF transmitter/antenna consists of 48 antenna elements arranged as a rectangular array of 8 columns by 6 rows (Figure 4), with a radiated power of 960 kW. Plans are to increase this ultimately to a 180-element system having a radiated power of

2

3.6 MW. In addition, the transmitter has a number of advanced features, making it an especially flexible and attractive instrument for the experimental research envisioned

Figure 4. View of the present 960 kW, 48 element, HF antenna array at Gakona. The planned full array will have 180 elements, and will radiate 3.6 MW.

under the program. These include an array bandwidth of approximately two octaves (2.8 MHz-10 MHz), a very wide and rapid scanning capability (±30° in all directions from zenith in 10 microseconds); any cross/circular or linear polarization, flexible control of transmitted waveforms, and the capability for two (simultaneous) frequency operation.

3. Diagnostic Instruments

The suite of on-site and off-site diagnostic instruments is extensive and diverse and plays an essential role during both active experiments employing the HF transmitter, as well as observing naturally occurring ionospheric processes when active research is not being conducted. In general, the diagnostics can be divided into two categories:

1. Instruments employed during active experiments to provide knowledge of ionospheric conditions prior to, during and after the operation of the HF transmitter. These include:
   Fluxgate Magnetometer
   Induction Magnetometer
   HF Ionosonde
   30 MHz Riometer
   Imaging Riometer
   Relative Total Electron Content – Transit Receiver
   Absolute Total Electron Content - GPS Receiver
   RF Spectrum Monitor

2. Instruments used during active experiments to assess the success of the research by measuring parameters associated with the specific heating experiment. These include:

> ELF/VLF Receivers
> Longwave Wideband Radiometer
> VLF D-Region Diagnostic System
> HF Stimulated EM Emissions Receiver
> 28 MHz Diagnostic Radar
> 139 MHz Coherent Backscatter Diagnostic Radar
> 449 MHz Incoherent Scatter Diagnostic Radar
> VHF Satellite Scintillation System (250 MHz)
> GPS Scintillation Monitor
> Optical Imager
> Near Infrared Imager
> Optical Telescope

Data collected from the instruments are processed and displayed at the site (Figure 5), and are provided in real time to other researchers via the internet (Figure 6). Many of the instruments are important diagnostic tools in their own right, having the capability to observe naturally occurring ionospheric processes when active research using the HF transmitter is not being conducted. For example, monitoring the outputs of these instruments on a day-to-day basis provides insight into the correlation between naturally occurring geophysical processes and radio wave propagation conditions (Figure 7).

There is no other facility in the world that has such a unique set of diagnostics with the capability to observe naturally occurring ionospheric processes when active research, using the HF transmitter, is not being conducted. As such they provide a major capability for observing space weather effects and the correlation between naturally occurring geophysical processes and radio wave propagation.

Figure 5. Diagnostic data display in the control room of the HAARP operations center.
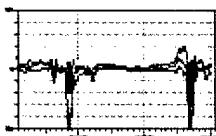
Magnetometer
Current Chart and Archives
Magnetometer Chain
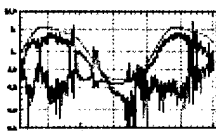
VHF Classic Riometer
Current Chart and Archives
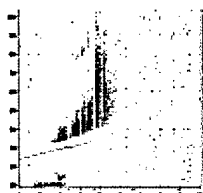
HAARP HF Ionosonde
Latest Ionogram
Ionosonde Home Page
Historical Time Series.

Induction Magnetometer
Current Chart
About the Induction Magnetometer
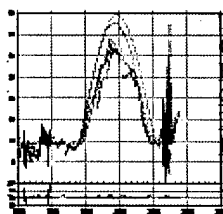
Total Electron Content (TEC)
Running TEC Chart
TEC Archive from GPS
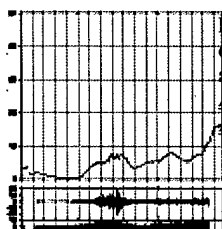
Latitude Scans of TEC and Scintillation
About TEC
Archive of Scans

TEC Tomography
Most Recent Image
Image Archive
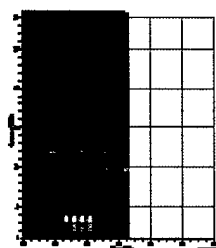
Spectrum Monitor Waterfall Charts
Current 1-30 Mhz chart
   Yesterday's chart
NCDXF Beacons chart
   Yesterday's Beacon chart
VHF waterfall chart 1
VHF waterfall chart 2
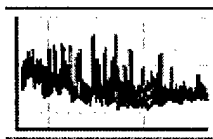
Spectrum Monitor Signal Strength Charts
WWV/WWVH (15 MHz)
WWV (20 MHz)
Int'l Broadcast 49m Band
Current Spectrum Monitor

HAARP Observatory Weather Station
Current Conditions
Running 36 hr Weather Chart
Archived weather data
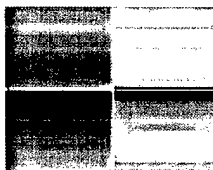
HAARP VLF Receiver
Chart Selector

HAARP All-Sky Imager
Latest All-Sky Image.
Image Catalog.

GPS Scintillation Charts from AFRL.
Ionospheric Scintillation Charts from AFRL.
Description of GPS Charts.

Figure 6. Example of diagnostic data available on the HAARP web site.

5
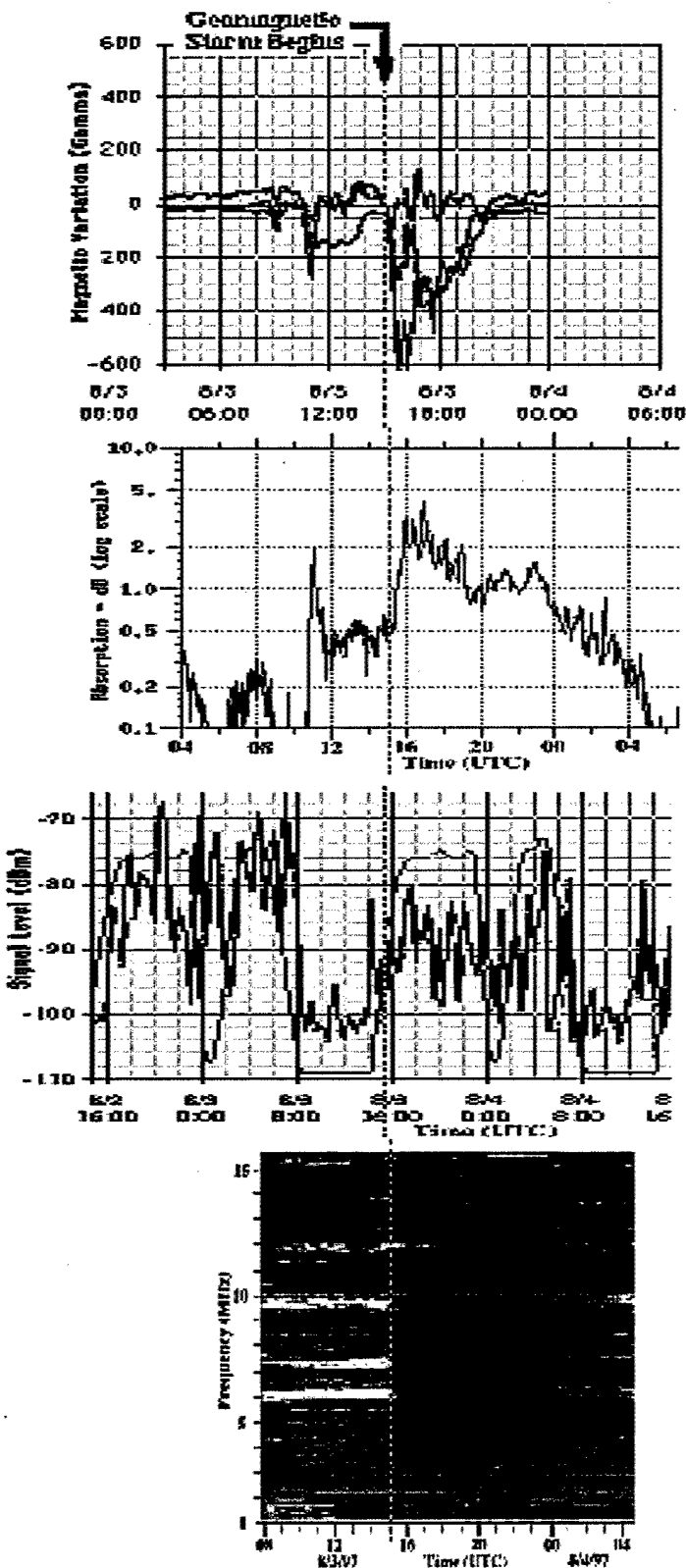
The magnetometer showed increased magnetospheric activity beginning at 1100 UTC with a small, short duration increase. This was followed by a return to nearly quiet conditions but a large dramatic increase in geomagnetic activity began again just after 1500 UTC and continued for several hours.

The 30 MHz riometer showed a large increase in overhead absorption, just after 1500 UTC, corresponding exactly with the large change observed in the magnetometer readings. Riometer absorption above 1 dB generally indicates poorer communications in the HF bands.

Signal levels observed at the HAARP site from the standard time and frequency stations WWV/WWVH near 15 MHz showed reduced strengths after 1500 UTC, in accordance with the magnetometer and riometer observations. The blue curve is the predicted level, the red is actually received.

The spectrum monitor, which records signal strengths over a wide band of frequencies, showed an abrupt loss of signals (communications blackout) throughout the entire HF band starting at 1500 UTC and lasting until early into the next day.

Figure 7. Effects of a coronal mass ejection from the sun on August 3, 1997, as observed on a number of diagnostic instruments at the HAARP Gakona facility.

6

4. Diagnostics Infrastructure
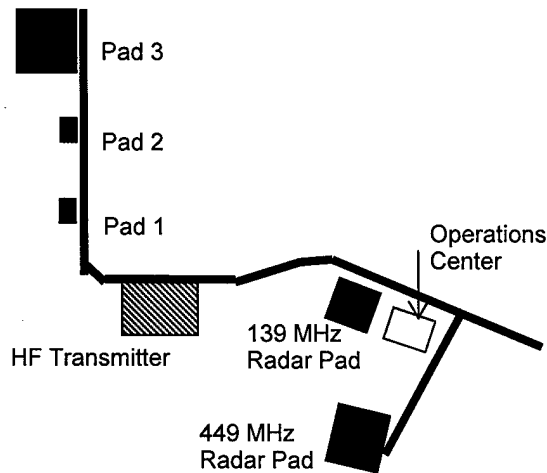
Figure 8. Current on-site diagnostic pads.

The Gakona site currently has pad and shelter space for diagnostic instruments in five areas, as shown in Figure 8. All the shelters are linked to the Operations Center through a high-speed fiber network. Pad 1 is 100 ft. x 100 ft. and includes the instrumentation shelter that houses the HF ionosonde and satellite receivers (Figures 9, 10 and 11). The HAARP ionosonde transmit antenna system is located on the left side of the site access road just before Pad 1. The four ionosonde receiving antennas are located just beyond Pad 1.
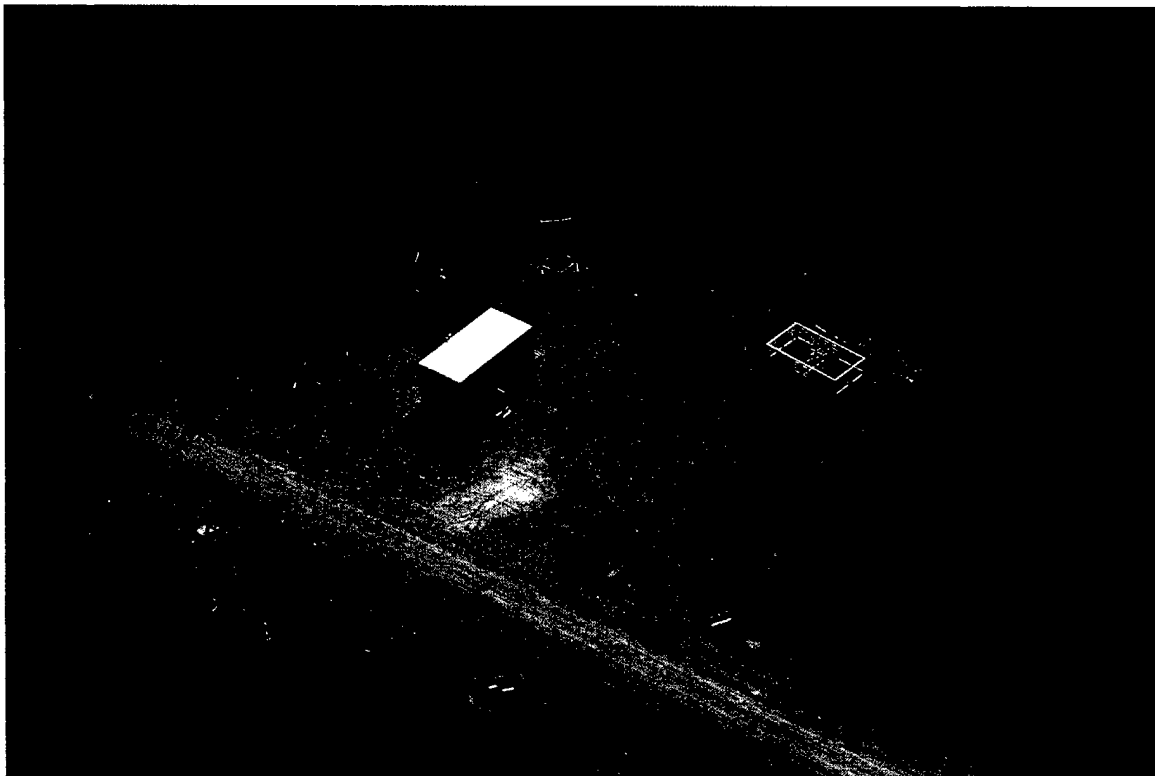
Figure 9. Pad 1 with instrumentation shelter along with the Transit antenna support structure on the right and GPS antenna support in the rear.
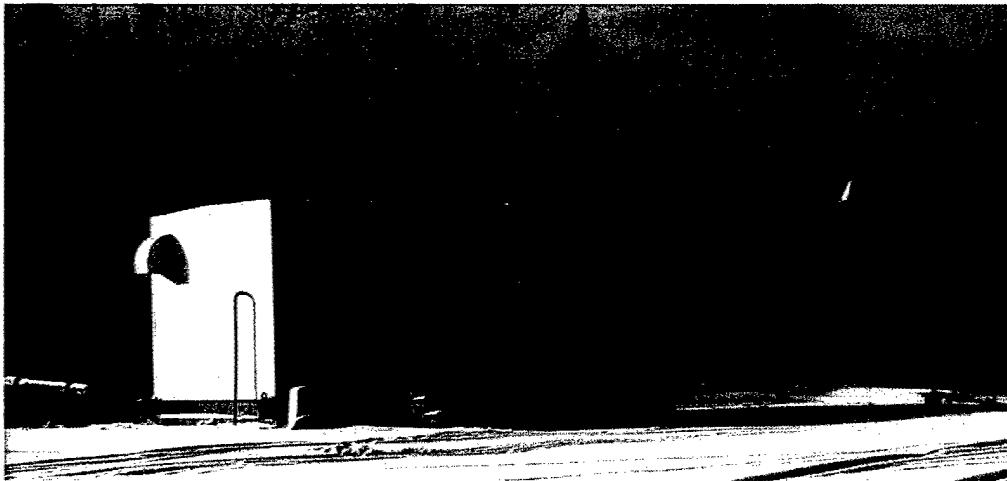
Figure 10. Pad 1 shelter with a GPS antenna in the background. . The shelter houses, ionosonde, scintillation and TEC diagnostic instrumentation.

Figure 11. Interior of Pad 1 Shelter. Transit and GPS receivers and data processors are in the foreground with the ionosonde at the end of the counter.

Pad 2 is also 100 ft. x 100 ft. It includes a small instrumentation shelter and an HF Spiracone receiving antenna (Figure 12) that is available for general diagnostic use. By switching the antenna connection at the base of the tower, either a vertical or horizontal pattern can be selected.

Figure 12. Pad 2 with HF Spiracone receiving antenna.

Pad 3 is 300 ft square and the quietest location on the HAARP facility for optical and rf measurements with two shelters available for instrumentation (Figures 13, 14 and 15). The Optics Shelter has three 1-foot domes for optical instrumentation and one 5-foot opening that can be equipped with either a sliding cover or a dome. The second shelter on Pad 3 supports the riometers, magnetometers and a VLF receiver.
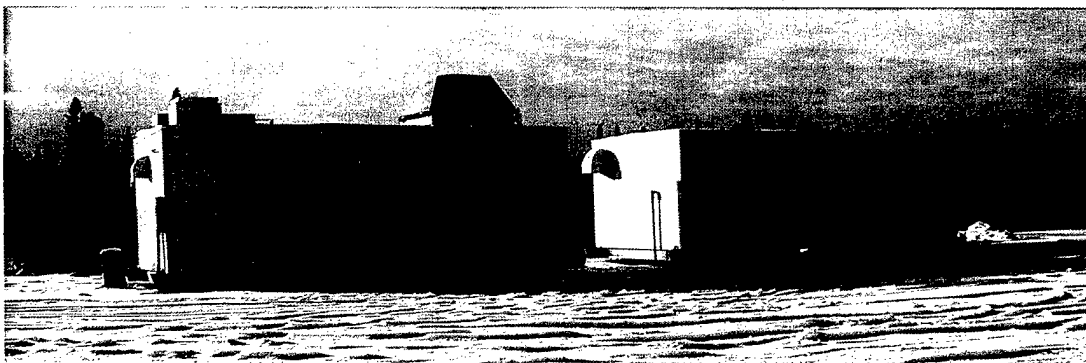
Figure 13. Pad 3 shelters contain optical instrumentation along with magnetometer, riometer and VLF instrumentation.

9
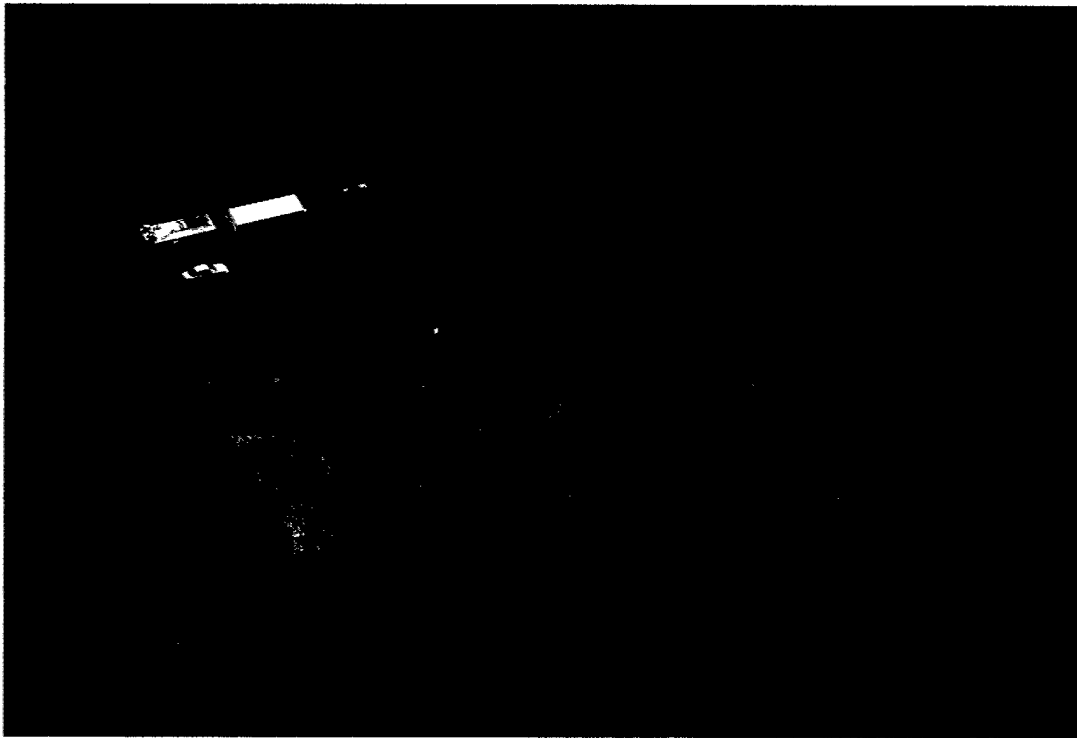
Figure 14. Pad 3 with the two instrumentation shelters. The 30 MHz Riometer antenna array is in the right corner of the pad and the Induction Magnetometer coils are in the center.

Figure 15. Interior of Pad 3 Shelter. The VLF receiver is in the foreground followed by the Fluxgate Magnetometer and 30 MHz Riometer.

The pad for the 139 MHz Coherent Backscatter Radar is located next to the Operations Center (Figure 16). The antenna array consists of 32 collinear, coaxial dipole rows supported on the black ABS pipe structure.

Figure 16. Shelter and antenna array for the 139 MHz Coherent Backscatter Radar.

In addition to the on-site instruments, many of the HAARP diagnostics are located off the facility, generally due to special geometry or noise considerations. For example:

1. ELF/VLF Receivers are installed 8 miles to the west of HAARP on the Richardson Highway and at the Poker Flat Research Range near Fairbanks.

2. An HF receiver for Stimulated Electromagnetic Emissions measurements has been operated near the center of Gakona, approximately 7 miles to the southwest.

3. The VHF Satellite Scintillation Monitor is installed in Slana, approximately 40 miles to the northeast.

4. Transit Satellite receivers for TEC and tomography measurements are located at Cordova and Delta Junction in addition to the receiver at HAARP

5. The three stations of the VLF D-Region Diagnostics System are located in Healy, Talkeetna and Dot Lake.

HAARP Diagnostic Instrument Summary Table

Diagnostic	Investigator	Description	Product/Measurement	Status
Fluxgate Magnetometer (On Site)	Dr John Olson Geophysical Institute University of Alaska	Triaxial, ringcore, fluxgate magnetometer with digital output: 0.1 nT sensitivity, 80,000 nT dynamic range	-Measurement of geomagnetic field and effects from aurora and IRI induced irregularities	Installed
Induction Magnetometer (On Site)	Prof. Kanji Hayashi University of Tokyo	Triaxial induction magnetometer: sensitivity of a few pT at 1 Hz, 2.5 Hz low-pass filter	- Measurement of magnetic variations due to short period magnetic pulsations - Measurement of lightning induced Schuman resonances	Installed
ELF/VLF Receiver (Off Site: Poker Flat Research Range and Gulkana Junction)	Dr. Davis D. Sentman Geophysical Institute University of Alaska	Two systems, specifically designed to monitor ELF and VLF signals generated in the ionosphere, each with a two-axis horizontal magnetic field receiver, software-selectable gain and filter stages and all-digital real-time signal processing	-ELF/VLF amplitude, phase and polarization	Installed
Longwave Wideband Radiometer (Off Site: Kangerlussuaq, Greenland)	Dr. Tony Fraser-Smith STAR Laboratory Stanford University	Receiver designed to monitor wideband background noise and ionospherically generated signals over the spectrum from 10 Hz to 50 kHz	-ELF/VLF signals in polar cap -Characterization of ELF/VLF/LF radio noise background	Installed
VLF D-Region Remote Sensing Receiver (Off Site: Healy, Dot Lake and Talkeetna, AK)	Prof. Umran Inan STAR Laboratory Stanford University	Three receiving stations, each monitoring the phase and amplitude of several VLF communication and navigation transmitters: data analyzed using three-dimensional propagation models.	-Location of auroral electrojet boundary -Infer D-region temperature and electron density profiles	Installed
HF Ionosonde (On Site)	Dr. Terence Bullett Air Force Research Lab Dr. Bodo Reinisch Univ. Mass. Lowell	Digisonde is a computer controlled vertical incidence HF ionosounder capable of real-time assessment and display	-IRI frequency management -Height profile of plasma (electron) density -Plasma drift velocities	Installed

HAARP Diagnostic Instrument Summary Table (Continued)

Instrument	Investigator / Organization	Description	Diagnostic Capabilities	Status
HF Stimulated Electromagnetic Emissions Receiver (Off Site)	Dr. Keith Groves, Air Force Research Lab; Dr. Frank Djuth, Geospace Research	HF receiver, tunable from 2 - 10 MHz with a 16 bit data acquisition system and spectrum analyzer: receiver operates in conjunction with the high power IRI transmitter.	-HF energy disposition/conversion -Magnetic field near reflection altitude -Infer HF-induced electrostatic wave modes	Available
Riometer (30 MHz) (On Site)	Mr. Jens Ostergaard, NorthWest Research Associates	30 MHz riometer with a 2x2 array of five element crossed Yagi antennas	-D and E region absorption	Installed
Imaging Riometer (On Site)	Dr. Ted Rosenberg, U. Maryland	1x16 array of riometer receivers operating at 38.6 MHz to provide 16 fan shaped beams in the magnetic N-S direction	-Spatial structure and temporal behavior of D and E region absorption -Altitude integrated electron temperature -Scaling between IRI parameters and electron heating	Installed
HF (28 MHz) Radar (Off Site)	Dr. Keith Groves, Air Force Research Lab; Dr. Frank Djuth, Geospace Research	28 MHz radar with centerline receive capability and high-speed data processor	-Mid-scale (6m) field aligned irregularities	Available
Coherent Backscatter Radar (139 MHz) (On site)	Dr. Keith Groves, Air Force Research Lab; Dr. Frank Djuth, Geospace Research	System utilizes an array of 32 colinear-coaxial antennas (gain > 30 dB) and a peak power of 32 kW. Independent phasing of 4 sub-arrays will permit beam-steering in the magnetic meridian.	-Ionospheric backscatter and power spectra from HF-induced ion turbulence and natural phenomena such as PMSE.	Installed
Incoherent Scatter Radar (On Site)	Dr. Brenton Watkins, Geophysical Institute, University of Alaska	Radar operating in the 450 MHz region based on the scattering of radio signals from density irregularities in the plasma.	-Electron and ion drift velocity -Electron density -Electron and ion temperature -Ion-neutral collision frequency -Neutral wind -Ionospheric conductivity and current density	Installation of initial panels scheduled

HAARP Diagnostic Instrument Summary Table (Continued)

Instrument	Provider	Description	Measurements	Status
VHF Scintillation Monitor (250 MHz) (Off Site; Slana, AK)	Mr. Robert Livingston Scion Associates Dr. Keith Groves Air Force Research Lab	Eight channel satellite signal receiving system using eight spaced helical antennas to sense both phase and amplitude fluctuations	-Velocity, shape and orientation of ionospheric structures -Assess artificial control of satellite links	Installed
GPS Scintillation Monitor (On Site)	Dr. Keith Groves Air Force Research Lab	Novatel single frequency GPS receiver	-GPS S4 as a function of elevation angles and time	Installed
Relative Total Electron Content (TEC) - Transit Receiver (On Site)	Dr. Edward Fremouw NorthWest Research Associates	NWRA Model ITS-10 Transit satellite receiver measures differential phase shift between the 150 MHz and 400 MHz signals.	-Latitudinal Scans of Relative Total Electron Content	Installed
Absolute Total Electron Content (TEC) - GPS Receiver (On Site)	Dr. Edward Fremouw NorthWest Research Associates	Ashtech Model Z-FX CORS GPS satellite receiver measures differential group delay and differential phase shift between the 1575-MHz (L1) and 1228-MHz (L2) signals.	-Absolute Total Electron Content	Installed
RF Spectrum Monitor (On Site)	Mr. Edward Kennedy Naval Research Lab	Computer controlled HP 8561E spectrum analyzer with whip and discone antennas	-Spectrum occupancy from 200 KHz to 1 GHz	Installed
Optical Telescope (On Site)	Elizabeth Gerkin Stanford University	Newtonian reflecting telescope (Meade Starfinder) with 16" aperture and f/4.5 Dobsonian mount	-Fine structure images of IRI induced airglow	Installed
Optical Imager (On Site)	Dr. Todd Pedersen Air Force Research Lab Peter Ning Scion Associates	Intensified CCD imaging system, 5 Rayleigh-sec sensitivity and real time digital image processing	-Images of IRI generated optical emissions -Images of auroral activity in vicinity	Installed
Near Infrared (NIR) Imager (On Site)	Dr. Paul Bernhardt Dr. Carl Siefring Naval Research Lab	Focal plane array with 2 inch f/1.2 collection optics and a 128x128 InGaAs photodiode array	-Images of SWIR from heater induced emissions -Spatial fluctuations in OH and O_2 from natural emissions	Available

ADDITIONAL POTENTIALLY AVAILABLE DIAGNOSTIC INSTRUMENTS

Diagnostic	Investigator	Description	Product/Measurement	Status
HF Vertical Sounder (College, AK)	US Air Force Air Weather Service	DISS computer controlled vertical incidence HF ionosounder capable of real-time assessment and display	-Height profile of plasma (electron) -Position, extent and velocity of irregularity structure	Installed
Magnetometer Chain	Geophysical Institute University of Alaska	Array of Narod Geophysics triaxial, fluxgate magnetometers across Alaska	-Geomagnetic field components	Installed
Riometer Chain		Array of La Jolla Sciences 30 MHz riometers across Alaska	-D and E region absorption	Installed
Optical Chain		Series of all sky optical imagers	-Distribution of auroral activity	Installed
HF SuperDARN Radar (Kodiak, AK)		8 to 20 MHz phased array radar	-Real time observations of ionospheric E- and F-region scatter	Installed
50 MHz Radar (Elmendorf AFB, AK)		50 MHz backscatter radar with fixed narrow beam antenna array	-Short scale (3m) field aligned irregularities	Installed

6. Individual Diagnostic Instrument Descriptions

1. Fluxgate Magnetometer
2. Induction Magnetometer
3. ELF/VLF Receiver
4. VLF D-Region Diagnostics System
5. ELF/VLF Wideband Radiometer
6. HF Ionosonde
7. 30 MHz Riometer
8. Imaging Riometer
9. 139 MHz Coherent Backscatter Radar
10. Relative Total Electron Content – Transit Receiver
11. Absolute Total Electron Content - GPS Receiver
12. 449 MHz Incoherent Scatter Diagnostic Radar
13. RF Spectrum Monitor
14. Optical Telescope
15. Optical Imager

1. Fluxgate Magnetometer

John V. Olson
Geophysical Institute, University of Alaska

The NAROD Fluxgate Magnetometer

Figure 1. Sensor head of the fluxgate magnetometer.

The Geophysical Institute at the University of Alaska Fairbanks supplies a fluxgate magnetometer for the measurement of the local magnetic field at the Gakona HAARP site. Manufactured by Narod Geophysics Ltd., the magnetometer is a high sensitivity, tri-axial ring-core design that samples the local field 8 times per second with 16-bit accuracy and has a resolution of approximately 10 picoTesla. Figure 1 shows the sensor head enclosure for the magnetometer. The sensor enclosure protects the sensors from the weather and is constructed to allow the sensors to be leveled and precisely oriented. The three sensors are oriented in a traditional, but non-standard, coordinate system in which the X-axis (sometimes labeled 'H') measures the north-south component of the local field, with north being positive. The Y-axis (sometimes labeled 'D') measures the east-west component of the field, positive eastward, and the Z-axis measures the vertical component, positive downward, forming a right-hand system of coordinates.

The sensor head is controlled by a computer system that establishes the working biases necessary to maintain high-resolution measurements during large field excursions. The computer also converts the sensor signals to physical units (nanoTesla) and digitizes the signals for output through a serial port. Data from the Narod serial port are read by software resident in a dedicated computer that serves to process and log the data to disk. The data are also displayed on the computer monitor as a check on magnetometer operation. Also logged with the magnetometer data is the GPS time in the form of an ASCII time stamp along with an IRIG-D slowcode that is treated as a data stream. This ensures correct timing of the data.

Data Collection and Internet Access

Finally, the data recorded to disk are shared with the HAARP data network and appear in real-time on the HAARP web site: http://www.haarp.alaska.edu. The data are also collected and are available through the Geophysical Institute Magnetometer Array (GIMA) web site: http://magnet.gi.alaska.edu. This web site includes the entire data set taken at Gakona as well as the other magnetometer stations operated by the Geophysical Institute. An example of the 24-hour plot available from the GIMA web site is given in Figure 2. There we show the fluxgate magnetometer data taken at Gakona on 13 October 1999. The mean is subtracted from each component and the components are displaced

vertically to reduce the overlap. During the interval shown there are large transients present produced by a series of auroral substorms.

Magnetometer trace in gammas for Gakona, AK Day 286, 1999
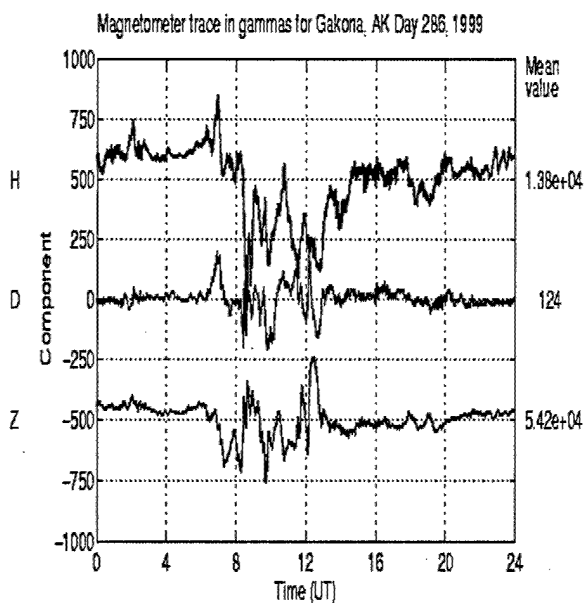
Figure 2. Fluxgate data from the HAARP site for October 13, 1999. The mean has been subtracted from each component and the axes are shifted to avoid overlap. The data show the presence of auroral substorms in the interval between 07:00 and 16:00 UT.

Modeling Ionospheric Currents

Taken together with data from the other magnetometers operated by the Geophysical Institute that span the State and the auroral oval, the equivalent ionospheric current density flowing in the overhead ionosphere can be estimated. With more information about the ionospheric conductivities, usually obtained from ionospheric models, estimates can be made of the field-aligned components of the currents as well. The Geophysical Institute maintains an interactive database that has the ability to make estimates of the equivalent ionospheric current flowing over Alaska and is available at http://gedds.pfrr.alaska.edu.

20

2. Induction Magnetometer

Kanji Hayashi
University of Tokyo

Introduction

The induction magnetometer detects temporal variation of the geomagnetic field based on Faraday's law of magnetic induction. This instrument is composed of three individual sensors. Each sensor is composed of a large number of turns of fine copper wire wound around a rod with high magnetic permeability. The sensitivity of each sensor is determined by the effective area of the detection coil, that is, the cross sectional area of each winding, and the number of turns, and by magnetic flux density threading the coil. The magnetic flux density is enhanced by a factor of approximately 1,000 by the high-permeability metal core.
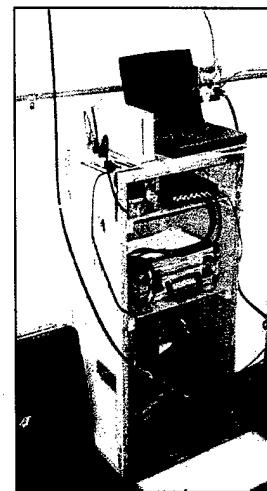

Figure 1. Data processing and recording equipment.

The HAARP Induction Magnetometer

The induction magnetometer installed at the HAARP site is designed to detect a signal level of a few picoTesla (pT) at 1 Hz. The overall frequency response of the magnetometer is shaped by Faraday's law at frequencies below 1 Hz and by active filters at frequencies above 1 Hz. Below 1 Hz the coil response is proportional to the time derivative of the magnetic field and thereby gives a response proportional to the frequency. Above 1 Hz, signals are suppressed by a low-pass filter with a corner frequency at 2.5 Hz. The filter response diminishes by 24 dB per octave above the corner frequency and thereby eliminates interference from 60 Hz radiation. The magnetometer sensors are aligned along the magnetic north, magnetic east and vertical directions to form an orthogonal measure of the derivative of the field. The sensor outputs are amplified by 40,000 and sampled at a 10 Hz rate with 16-bit resolution in a full scale of 10 Volts.

Typical signals

Magnetic field variations of interest in this program are those induced by electric currents in the ionosphere. The major signal categories detected by the induction magnetometer are short period magnetic pulsations such as Pc1, Pc2, Pc3, PiB, and PiC in a frequency range above a few tens of milliHertz. Among these, the induction magnetometer most efficiently detects Pc1 waves in the frequency range from 0.1 Hz to 3 Hz. Pc1 signals are the result of ion-cyclotron radiation generated near the equatorial plane of the outer magnetosphere that make their way to the ionosphere guided by the magnetic lines of force. In addition, signals generated in the atmosphere that are caused

by lightning discharges, the Schuman resonances, are also detected and sometimes become strong enough to mask signals from the ionosphere.

The image below is a 24 hour time-frequency spectrogram, which shows the frequency content of signals recorded by the HAARP Induction Magnetometer. This instrument measures temporal variations in the geomagnetic field in the ULF (ultra-low frequency) range of 0-5 Hz. The spectrogram images are produced by computing the PSD (power spectral density) of successive 102.4-second segments of timeseries data, and plotting these spectra as color/intensity slices along a 24-hour scale. Figure 2 shows an example of narrowband PC1 signals, while Figure 3 gives an example of wideband ULF noise during a magnetic substorm.
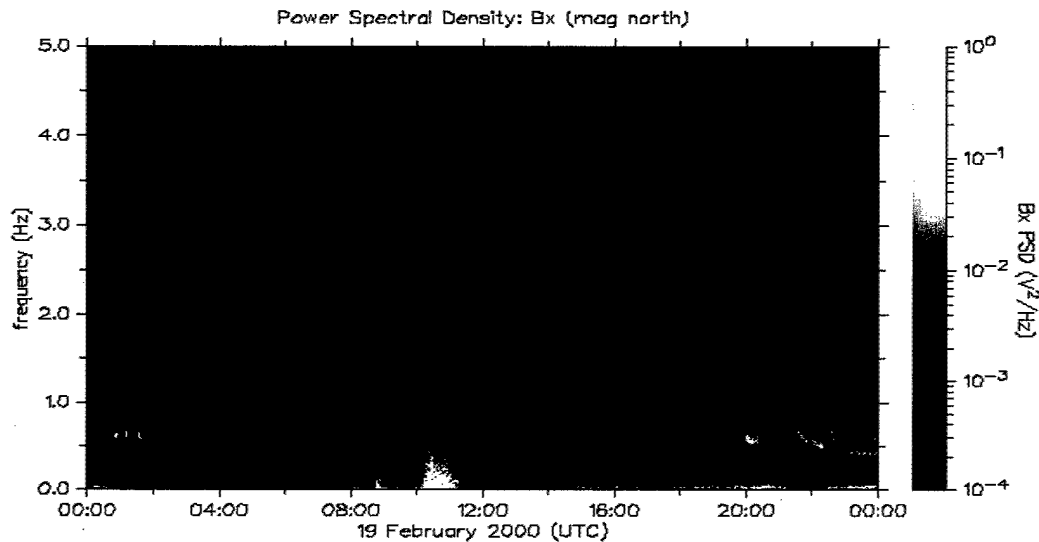

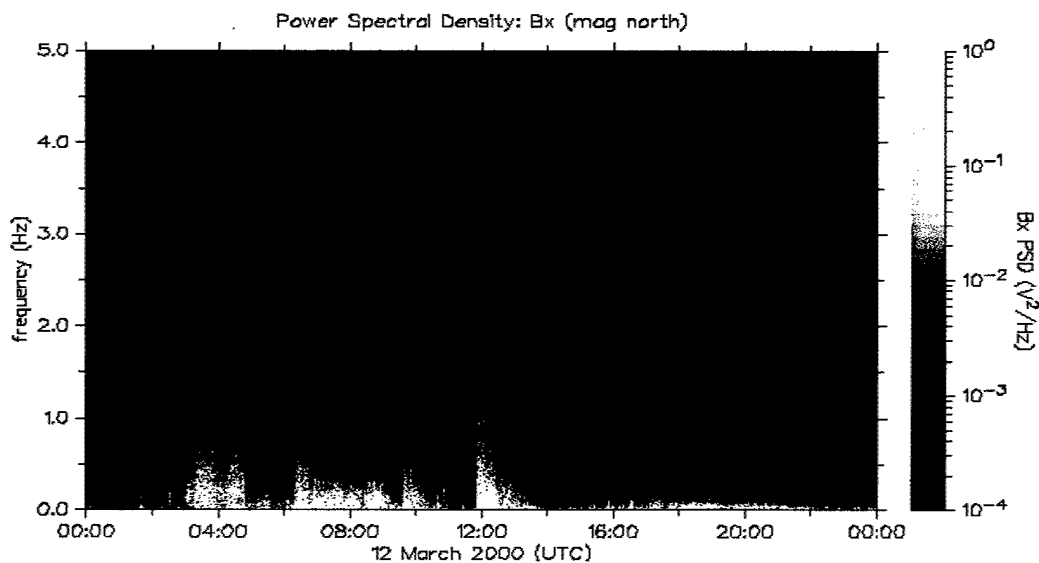*Figure 2. Example of spectrogram showing narrowband PC1 signals.*

Figure 3. Example of spectrogram showing wideband ULF noise during a magnetic substorm.

22

3. ELF/VLF Receiver

D.D. Sentman
Geophysical Institute, University of Alaska

Objective

ELF/VLF diagnostic measurements will be used to monitor the effects of HF modulation of the Polar Electrojet (PEJ) at ELF and VLF frequencies. The measurements are made at two locations. One site close (~10 km) to HAARP is located north of Gakona and used to monitor the near field ELF/VLF emissions. A second site is located at Poker Flat at a distance of 350 km from HAARP.

Figure 1. Sensors, sensor box, and instrument trailer at Gakona ELF site.

Instrument

The sensors are electrostatically shielded induction coils that are optimized for operation in the frequency band 3-12,000 Hz and measure the orthogonal horizontal components of the magnetic field. Sensor outputs are delivered via optical fiber to a real-time data acquisition and analysis system. Figure 1 shows the sensors and instrument trailer at Gakona. The real time computer systems convert the signals to digital form at 27.8 kHz using GPS synchronization, and perform various signal conditioning and filtering operations, and compute a variety of diagnostic information. These include synchronous detection of HAARP modulation frequencies, waveform stacking, and dynamic frequency-time spectra and amplitude distributions. The system can be remotely configured and administered over the Internet.
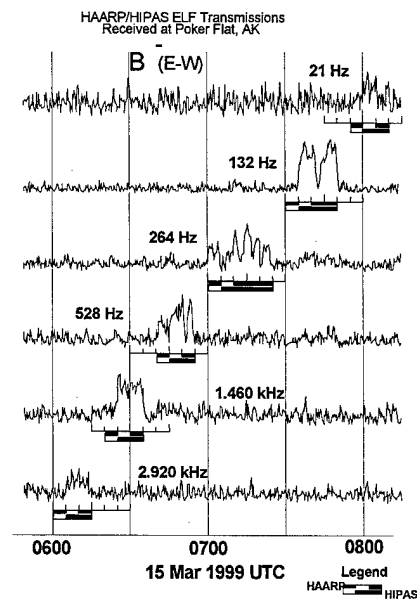

Figure 2. ELF and VLF signals generated by HAARP and HIPAS by means of HF modulation of the auroral electrojet. The traces are 20-second integrations at the indicated frequencies.

Data Sample

Figure 2 shows a sample of synchronously detected ELF emissions recorded at the Poker Flat site on the night of 15 March 1999. The experiment utilized both HAARP and HIPAS to investigate

23

interference effects between ELF emissions generated from the two transmitters. Weak to moderate signal strengths were detected across all ELF transmission frequencies, ranging from 21 – 2940 Hz.

The principal components of the HAARP ELF/VLF detection system are summarized below.

HAARP ELF/VLF Systems

Analog System

Component	Description
• Sensors	EMI BF-10 Induction Coils 3-12000 Hz; sensitivity $1 \text{ pT}/\sqrt{Hz}$
• Receiver Hardware	Fiber optic connectors sensor-receiver, 20-bit, 48 kHz
	DSP 60 Hz rejection comb filter, 16-bit, 44.1 kHz
• Time Standard	Spectrum Time Machine GPS

Data Acquisition System

Component	Description
• Digital Platform	PC, 350 MHz PII
• OS	Microsoft Windows NT 4.0 Server
• A/D Subsystem	Data Translation DT-3001 12-bit ADC/DAC/CTR; external triggering from GPS source
• Network	Ethernet, TCP-UDP/IP
• Software Architecture	COM/DCOM multithreaded client-server; real-time data server feeding client analysis modules
• Data Base Format	NetCDF, HAARP conventions
• Remote Control	Various; principally pcAnywhere

Software Modules

Module	Function	Status
• Data Server	Sample data at 27.8 kHz, low pass filter and sub-sample into 4 user selectable filter banks	Operational
• Synchronous Detection	Detect and log amplitude and phase narrow band signals at up to 8 user specified signal and 8 noise frequencies 3-10000 Hz with absolute phase stability < 1 µs; arbitrarily long integration intervals; linear and non-linear detection options	Operational
• Spectra	Compute and log dynamic spectra 3-200 Hz	Operational
• Time Series	Log sampled data	Operational
• Q-Burst	Detect and log ELF transients	Operational
• Amplitude Probability Distributions	Assemble and log amplitude probability distributions; used as input to non-linear synchronous detection module	Under development
• Stack	Assemble and log stacked periodic waveforms of arbitrary period	Under development
• Multisite	Collection of real-time ELF data from multiple remote sites for ELF phased array and spatial differential signal studies	Planned

4. VLF D-Region Diagnostics System

U. S. Inan, T. F. Bell, M. Johnson, M. Chevalier, M. Demirkol, and R. Moore
STAR Laboratory, Stanford University,

Introduction.

VLF signals propagating in the Earth-ionosphere wave guide are scattered by localized disturbances in the D-region of the ionosphere. At the receiver, the scattered signal adds to the direct signal, producing changes in the phase and amplitude of the total received signal.

The localized D-region disturbances can be produced by a variety of mechanisms, such as energetic particle precipitation, gravity waves, heating by lightning, and heating by powerful HF transmitters such as HAARP, as indicated in Figure 1.
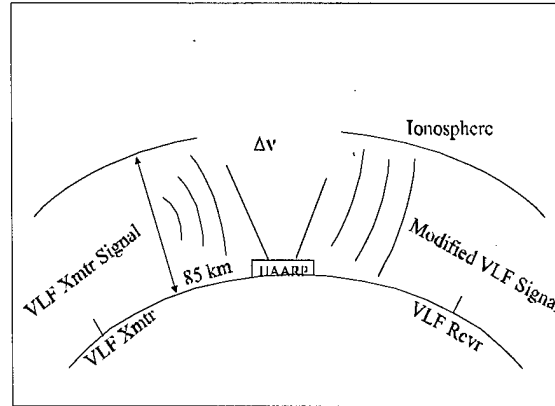

Figure 1. Subionospheric VLF signals propagating in the Earth-ionosphere waveguide are scattered by localized D region disturbances, modifying the total signal received at a distant site.

In the case of HAARP, the VLF wave scattering occurs because the HAARP HF waves heat the electrons in the ionosphere and change their collision frequency, thereby changing the conductivity of the medium. Thus the HAARP-induced phase and amplitude change in each VLF signal propagating near the HAARP site can be used to characterize the heated electron collision frequency profile in the ionosphere over HAARP.

The VLF D-region diagnostics system.

The VLF D-region diagnostics system consists of three VLF receiving systems plus a number of computer codes used in data analysis and interpretation. Each receiving system is sited at a High School located within 500 km of the HAARP facility. The High Schools, those at Healy, Talkeetna, and Dot Lake, were chosen because the local science teacher and students exhibited a high degree of interest in the project and the scientific data and were willing to provide the small amount of maintenance the systems require.
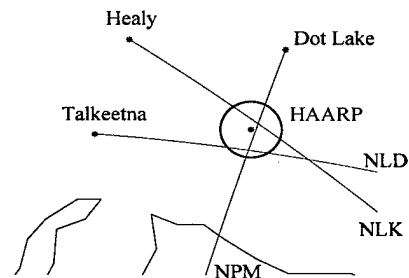

Figure 2. Disposition of the three D- region diagnostics systems with respect to the HAARP facility.
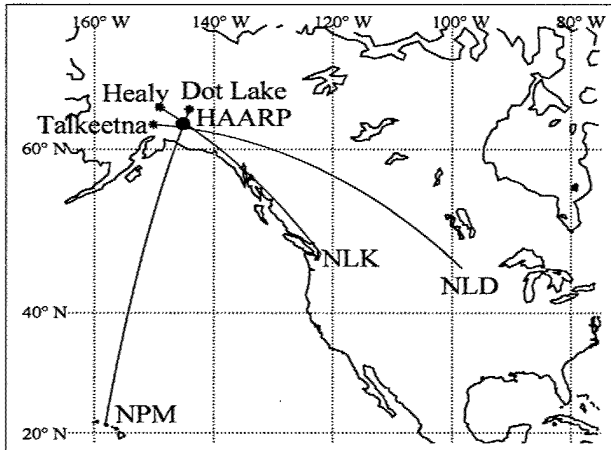
Figure 3: Propagation paths of the NLK, NPM and NLD signals to HAARP.

The receiving system deployment with respect to HAARP is shown in Figure 2. The Healy system monitors the phase and amplitude of the NLK signal from Washington, the Talkeetna system monitors the NLD signal from North Dakota, and the Dot Lake system monitors the NPM signal from Hawaii. The total propagation paths of these signals are shown in Figure 3.

Each receiving system consists of a loop antenna and preamplifier that respond to the subionospheric VLF waves and relay an amplified analog signal to the main electronics box where the signal is filtered and read by the system computer through an A/D card. The amplitudes and phases of the NLK, NPM, and NLD signals are then extracted. The data are synchronized in time with the other sites by means of a GPS receiver. Data are generally stored as acquired and sent to Stanford over the Internet during a one hour period during the day. Data can also be distributed over the web to interested parties in near-real time whenever necessary.

An example of diagnostics system data.

Figure 4 shows a typical example of data from the VLF D-region diagnostics system obtained during the March 1999 HAARP/HIPAS campaign. The   panel shows the amplitude of the NLK signal as received at Healy on March 9, 1999. At this time the
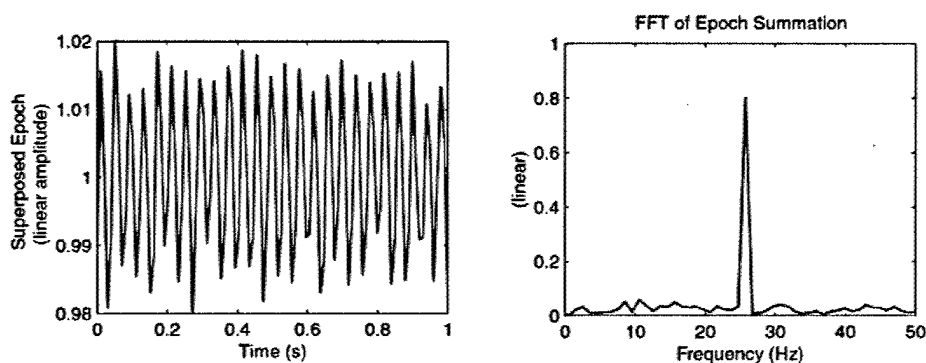
Figure 4. NLK amplitude at Healy on March 4 1999. Left-hand panel shows 25 Hz modulation of the NLK amplitude. The right-hand panel shows FFT of NLK amplitude.

HAARP HF output was a 100% amplitude modulated square wave at 25 Hz. The 15 minute data block was analyzed using a superposed epoch technique to produce a single

26

data block of one second duration. A 25 Hz amplitude modulation can be seen clearly in the data.

Inversion of the amplitude and phase data

In general, the three station amplitude and phase data will be used in conjunction with a computer-based inversion algorithm to determine the collision frequency profile in the D-region above HAARP during HF heating experiments. This algorithm was developed as part of the PhD thesis work of M. Demirkol of STAR Laboratory.

5. ELF/VLF Wideband Radiometer

A. C. Fraser-Smith
Stanford University

Instrumentation

The wideband radiometer consists of two dual-channel receivers, each with two crossed loop antennas. One of the receivers has a response covering the frequency range 10–500 Hz (ELF) and the other covering the range 200–32,000 Hz (VLF). A bank of narrow-band (5% bandwidth) filters is used to monitor the noise present at 16 selected frequencies distributed approximately uniformly in a logarithmic sense through the overall frequency range of operation. These frequencies (see Table 1) were carefully chosen to avoid harmonics of the 50 Hz and 60 Hz power line frequencies. The output of these filters is continuously sampled and a variety of statistical quantities calculated and recorded digitally on magnetic tape, along with samples of the raw data from the filters (typically one sample/second for all 16 filters).
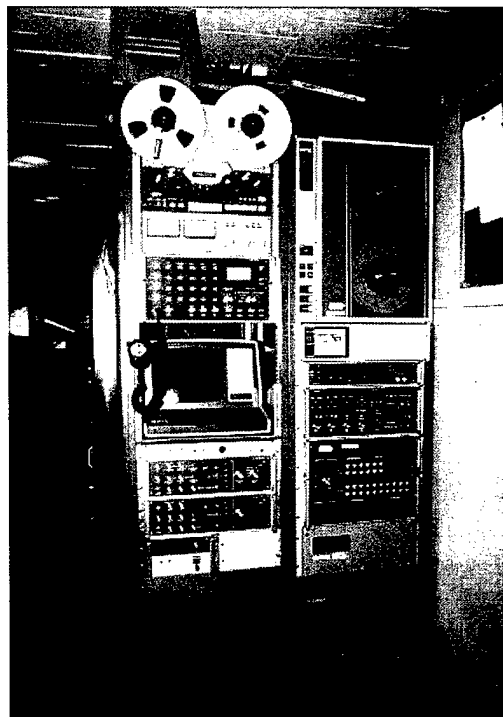
In addition to the data from the narrow band filters, broad-band ELF data, sampled at a rate of 1000 samples per second during scheduled synoptic recording intervals (currently one minute each hour), are also recorded on the digital tape. These data can be converted to spectrograms and they provide an essential check on the operation of the narrow-band filters and their associated measurements. A similar synoptic picture of activity in the VLF range is provided by analog recordings of the range 200–32,000 Hz. These broad-band measurements can also be conducted under operator control, thus providing the radiometers with the capability to participate in measurement campaigns (such as those organized by HAARP) at any time. See *Fortnam* [1985] and *Fraser-Smith and Helliwell* [1985] for a more complete description of the radiometers. Their measurements have been described in many publications and reports, some of which are listed without citation in the attached reference list.

TABLE 1. Center frequencies and bandwidths for the 16 narrowband channels of the ELF/VLF radiometer.

Channel	Center Frequency	Bandwidth (5%)
ELF System	Hz	Hz
1	10	0.5
2	30	1.5
3	80	4.0
4	135	6.75
5	275	13.75
6	380	19.0
VLF System	kHz	Hz
1	0.5	25.0
2	0.75	37.5
3	1	50
4	1.5	75
5	2	100
6	3	150
7	4	200
8	8	400
9	10.2	510
10	32	1600

Simultaneous Observations at Stanford and Thule

One of the possible applications of the HAARP facility is the generation of ELF/VLF radio waves by modulation of the auroral electrojet currents flowing in the ionosphere above Alaska. Although estimates of the orientation and strength of the electrojet can be made, it is not at all obvious at this time how the strength of the ELF/VLF waves will vary at locations distant from HAARP. Figure 1 shows the desirable locations of the Stanford/Thule radiometer pair for diagnostic measurements.
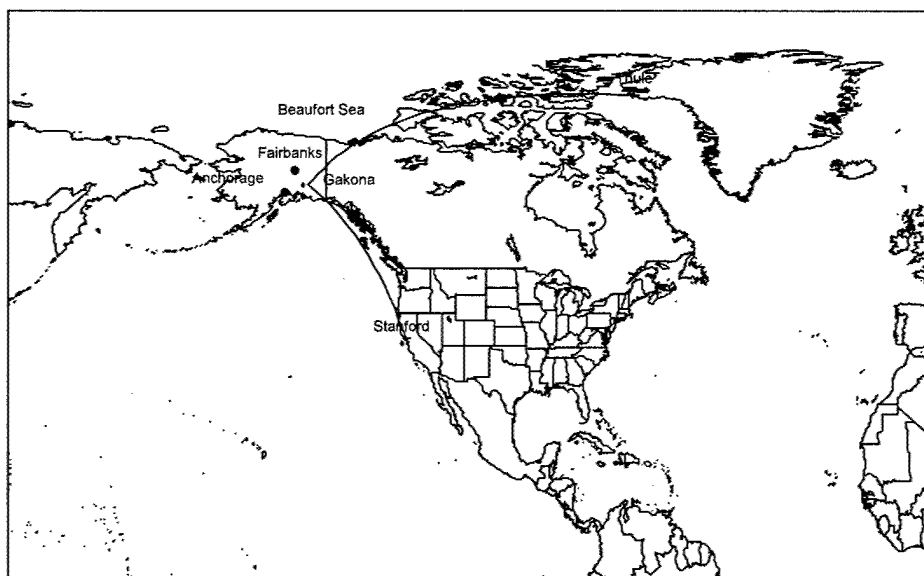

Figure 1. The locations of the Stanford and Thule radiometers for diagnostic measurements on any ELF and VLF signals produced during HAARP experiments.

LF Noise Measurements

One of the most important features of the HAARP facility from the point of view of those involved with low-frequency communications if the possibility of producing ELF electromagnetic signals for research – currently there are only two operational ELF transmitters in the world and both are in use for military communications and thus unavailable for research. It is in this context that Figure 2 shows an illustrative spectrogram of the lower ELF radio noise occurring at Sondrestromfjord, Greenland, during January 1990. There are many interesting features in this noise and one not-so-interesting feature – the ever-present interference at 60 Hz, 50 Hz, and harmonics of these frequencies, from electric power distribution systems (Sondrestromfjord, nevertheless, is a relatively low-noise measurement site). Two of the interesting features are the Schumann resonances that can be seen occurring in the frequency range 7–50 Hz and the strong 82 Hz signal from the Russian ELF transmitter located on the Kola peninsula. See *Fraser-Smith and Bannister* [1998] for further details.
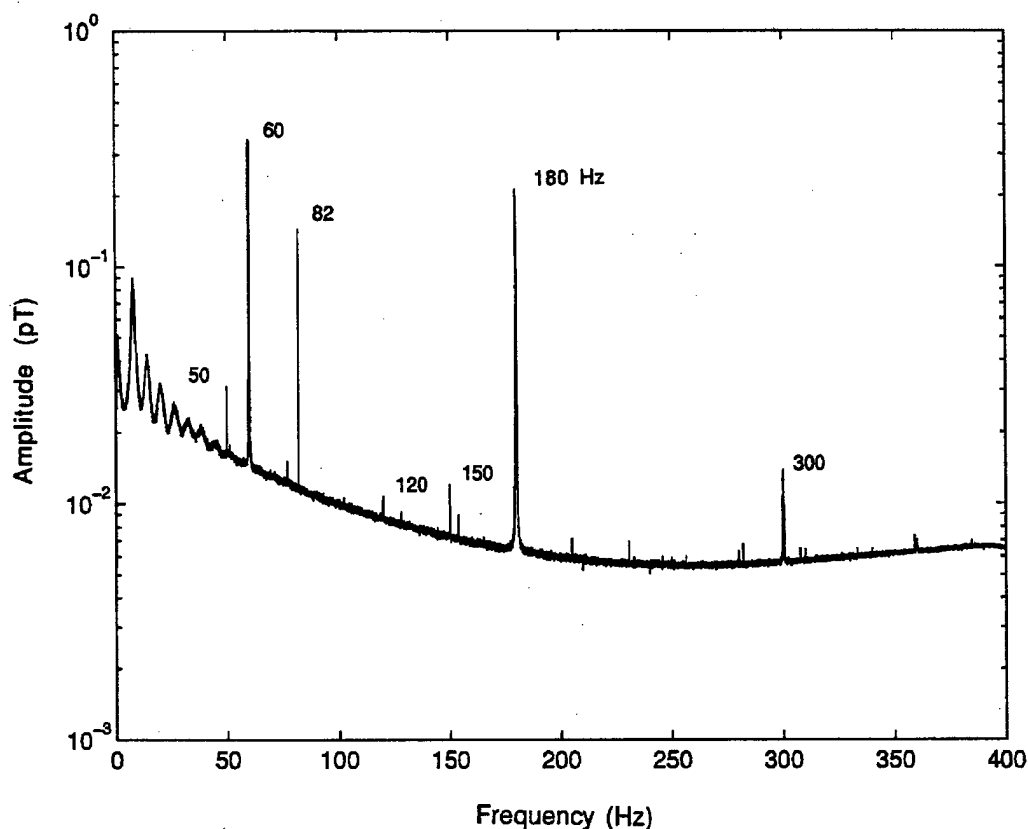

Figure 2. Average amplitude spectrum of the lower ELF radio noise at Sondrestromfjord, Greenland, during January 1990. The average spectrum is computed from the 1185 1-min synoptic recordings taken twice per hour that contained 82-Hz transmissions; the total possible number of these 1-min recordings during January is 1488.

References

Chrissan, D. A., and A. C. Fraser-Smith, "Seasonal Variations of Globally-Measured ELF/VLF Radio Noise," *Radio Science,* **31**, 1141–1152, 1996.

Chrissan, D. A., and A. C. Fraser-Smith, "A Comparison of Low-Frequency Radio Noise Amplitude Probability Distribution Models," *Radio Sci.,* **35**, Jan. – Feb. 2000

Fortnam, B.R., *An automatic system for global monitoring of ELF and VLF radio noise phenomena, Tech. Rept. E450–1,* 107 pp., STAR Laboratory, Stanford University, June 1985.

Fraser-Smith, A.C., and R.A. Helliwell, "The Stanford University ELF/VLF radiometer project: Measurement of the global distribution of ELF/VLF electromagnetic noise," Proc. 1985 IEEE Internat. Symp. On Electromag. Compatibility, *IEEE Cat. No. 85CH2116--2,* 305–311, 1985.

Fraser-Smith, A. C., P. R. McGill, R. A. Helliwell, and Sibylle Houery, *Radio Noise Measurements in the Long-Wave Band at Thule, Greenland,* Final Technical Rept. RADC-TR-89-94, Rome Air Development Center, Griffiss Air Force Base, N.Y., 74 pp., August 1989.

Fraser-Smith, A. C., P. R. McGill, A. Bernardi, R. A. Helliwell, and M. E. Ladd, "Global Measurements of Low-Frequency Radio Noise," pp. 191–200, *Environmental and Space Electromagnetics,* Ed. H. Kikuchi, Springer-Verlag, Tokyo, 1991.

Fraser-Smith, A. C., and J. P. Turtle, "ELF/VLF Radio Noise Measurements at High Latitudes during Solar Particle Events," paper presented at the 51st AGARD–EPP Specialists' Meeting on "ELF/VLF/LF Radio Propagation and Systems Aspects," Brussels, Belgium, 28 September – 2 October, 1992, published in *AGARD Conference Proceedings No. 529,* pp. 16-1 to 16-8, May 1993.

Fraser-Smith, A. C., and R. A. Helliwell, "Overview of the Stanford University/Office of Naval Research ELF/VLF Radio Noise Survey," pp. 502–509 in *Proc. 1993 Ionospheric Effects Symposium,* Ed. J. M. Goodman, SRI International, Arlington, Virginia, 1994.

Fraser-Smith, A. C., Low-Frequency Radio Noise, Ch. 12 in *Handbook of Atmospheric Dynamics,* Vol. 1, pp. 297–310, Editor H. Volland, CRC Press, 1995.

Fraser-Smith, A. C., and P. R. Bannister, "Reception of ELF signals at antipodal distances," *Radio Science,* **33**, 83–88, 1998.

6. HF Ionosonde

Bodo W. Reinisch[1], D. Mark Haines[1] and Terence W. Bullett[2]

[1]University of Massachusetts Lowell, Center for Atmospheric Research

[2]Air Force Research Laboratory, Hanscom Air Force Base

Principles of Ionospheric HF Sounding

Monitoring the large variations in electron density in the earth's ionosphere requires remote sensing techniques. Since the early experiments by Breit and Tuve [1926], high-frequency (HF) sounding with ionosondes has provided a wealth of information on the structure and dynamics of the ionosphere. Incident radio waves are reflected back to the transmitter at each location where the sounding frequency equals the plasma frequency f_p,

Figure 1. DPS transmit antenna.

$$f_p^2 = Ne^2/4\pi^2 m\varepsilon_0$$

(N = electron density, e = electron charge, m = electron mass, ε_0 = free space permittivity) and where the wave normal **n** is parallel to the electron density gradient δN. Actually there exist different wave modes, the O, X and Z modes. Only the O mode is reflected at $f_p = f$, while the other modes are reflected at slightly different plasma frequencies (Reinisch et al., 1997). The delta or rhombus transmitter antennas typically used for vertical sounding have wide beamwidths that illuminate an area of several hundred kilometers diameter in the ionosphere. This can lead to many reflection points fulfilling the condition **n** × δN = 0, unless the plasma distribution is spherically symmetric (i.e. concentric with the Earth's surface) in which case there exists a single reflection point directly overhead. Advanced digital ionosondes (Reinisch, 1996) identify and measure the multitude of echoes arriving simultaneously from different directions, determine the overhead echo traces for real time calculation of the vertical electron density profiles, and use the location and Doppler shifts of the off-vertical echoes to specify the structure and dynamics of the plasma distribution.

The DPS at Gakona

In the auroral zone where the HAARP facility is located, ionospheric conditions are very dynamic and localized so even nearby sounders in Anchorage and Fairbanks cannot give a reliable estimate of conditions at HAARP. Therefore it was decided early in the planning stages that an on-site ionospheric sounder would be included. The Digisonde Portable Sounder, or DPS, was installed near the heater to support the
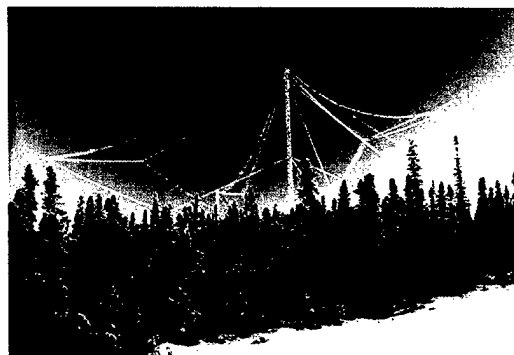
frequency management of the heater and to provide preliminary ionospheric diagnostics. A detailed description of the system is given on the University of Massachusetts Lowell website http://ulcar.um.edu. The DPS simultaneously measures seven observable parameters of the reflected signals received from the ionosphere:

1) frequency, 2) virtual range/ height , 3) amplitude, 4) phase, 5) Doppler shift and spread, 6) angle of arrival, and 7) wave polarization.

These parameters are displayed in a virtual range vs sounding frequency frame called an ionogram. The virtual range R' is defined as $R' = \frac{1}{2} c\, t_e$ where t_e is the echo delay time, and c the speed of light in free space. To identify the different wave modes, the DPS transmit and receive antennas are circularly polarized. The X mode waves have right-hand circular polarization with regard to the geomagnetic field, while both the O and Z mode waves have left-hand circular polarization. The true height inversion program NHPC (Huang and Reinisch, 1996) in the DPS calculates the vertical electron density profiles from the measured virtual echo traces h'(f).
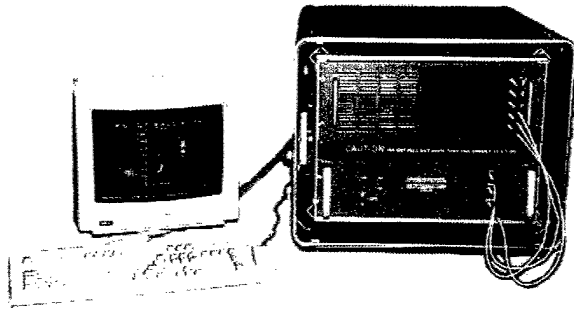

Figure 2. Digisonde Portable Sounder.

The main DPS specifications are summarized in Table 1. The DPS compensates for a low power transmitter (200 W vs. ~10 kW for other ionosondes) by employing intrapulse phase coding, digital pulse compression, and Doppler integration as its digital signal processing techniques (Haines, 1994). The DPS Gakona transmit antenna is shown in Figure 1. The central 30 m tower supports two orthogonal delta antennas driven by two transmitters that are 90° out of phase. The integrated transceiver package, shown in Figure 2, is housed in the diagnostics shelter, Figure 3. A crossed-loop receiving antenna is included in Figure 4. The receiving array, consisting of four antennas, is used for interferometry to determine the echo locations of the Doppler shifted echoes.

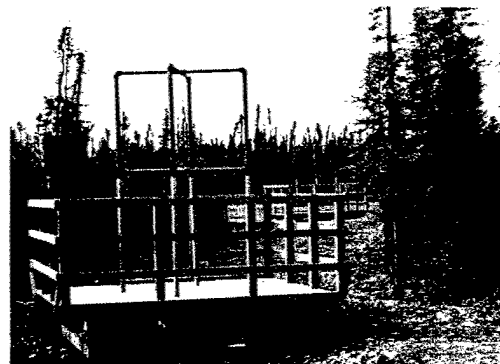*Figure 3. Diagnostics shelter containing DPS transceiver.*

Figure 4. Crossed-loop receiving antenna.

DPS Data Products

All DPS data are locally stored on a Jaz removable cartridge but are also available on the Internet for real time access: http://137.229.36.56/. The data for the two operational modes, ionograms and skymap/drift data, are stored in binary format. The
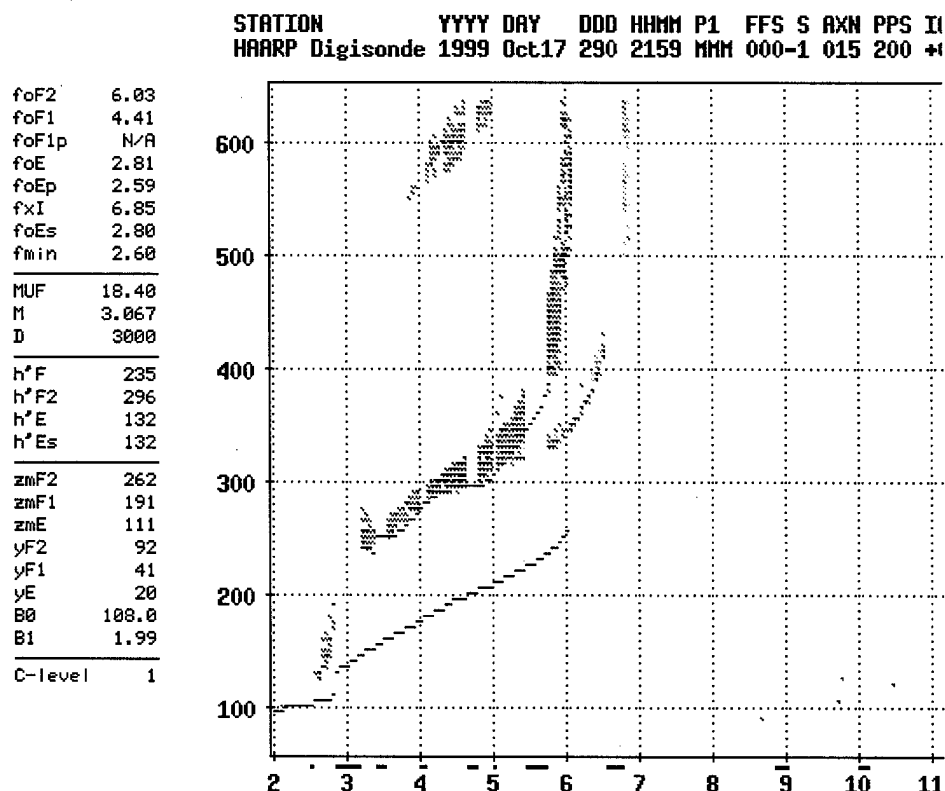

Figure 5. Gakona ionogram with autoscaling.

scaled ionogram characteristics and density profiles are in an ASCII format file using the URSI recommended SAO format. This file contains 43 different ionospheric characteristics scaled from the ionogram. The SAO format is described in http://ulcar.uml.edu/~iag/SAO-4.htm. The ionogram in Figure 5 shows the raw ionogram data combined with the results of the autoscaled data generated by the ARTIST software residing in the DPS.

This quiet daytime ionogram shows the O echo traces (red) for the E, F1 and F2 layers, and the X trace (green) near the F2 cusp. The black dots at the leading edge of the O trace are the autoscaled h'(f) values. The other (lower) black curve is the electron density profile represented here as h(f$_p$). The more important characteristics like foF2, foF1, etc. are displayed on the left of the ionogram. The letter p indicates model prediction for this time and location. By superimposing the autoscaled traces onto the measured ionogram, the user can judge the performance quality of the autoscaling. The ARTIST program also specifies a confidence level indicator (C-level, 1= high, 5=low) that was set to 1 for this ionogram. The red bars along the frequency axis indicate "restricted" frequencies, i.e., frequencies without transmission because of operating

35

restrictions issued by the Air Force frequency allocation agency. Although ARTIST scaled successfully through these gaps for the ionogram in Figure 5, these restricted frequencies are often the cause serious autoscaling mistakes.

For diagnostic purposes, the Digisonde skymaps will be very useful in monitoring changes in the plasma distribution of the heated region. Figure 6 shows a skymap for f = 2.5 MHz at 5 January 2000, 5:48 UT. The red and blue dots are the locations of the reflection points with negative and positive Doppler velocities. Clearly there exist two reflection regions, one overhead and another at ~20°in the southeast. The distribution of Doppler frequencies indicates that the plasma moves in the southwest direction. The off-line DDA software can calculate the drift velocity vector (Scali et al., 1997).
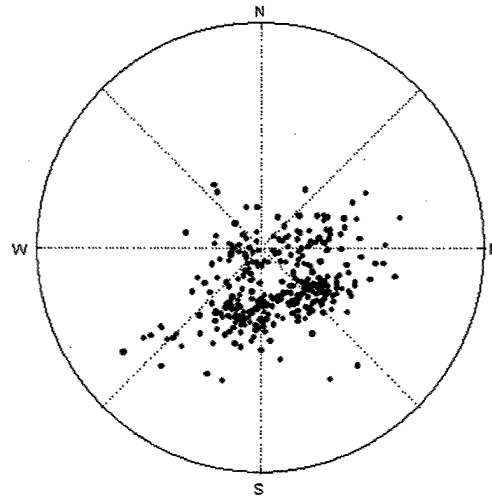
Figure 6. Gakona Skymap, f = 2.5 MHz at 5 January 2000,

The Digisonde Web page provides the user with a chart showing availability of data for public access. Scaled ionogram data that is stored on the system (SAO files) is available for download or to be plotted by a Java applet launched in the user's Web browser. These plots, like the one in Figure 7, are useful for viewing long-term trends in the scaled parameters.

Figure 7. Example of data available on Digisonde web-page.

Table 1. DPS General Specifications.

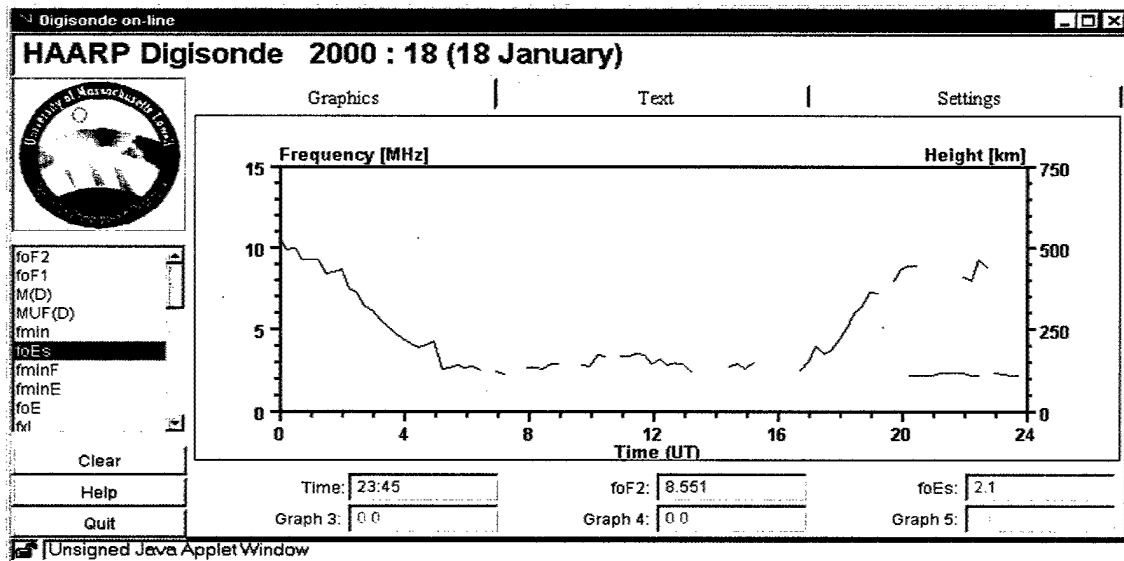| RECEIVER	
Frequency Range	1.0 – 40 MHz (all modes of operation)
Bandwidth	34 kHz @ 6 dB (for 5 km pulse resolution)
Noise Figure	11 dB (at receiver antenna preamplifier)
Receiver Sensitivity	-126 dBm into main chassis. Sensitivity is greater at preamplifier (amount depending on fixed gain setting)
Spurious Free Dynamic Range	>80 dB instantaneous >120 dB total operating range including gain control
Output	12-bit quadrature samples (16-bit after pulse compression)
RF Transmitter	
RF Power	Two transmitters with 150 W each
Frequency Sweep	1-40 MHz, Start, stop and step size settable to 1 kHz
Ionogram Sweep Time	Standard VIS ionogram 100 sec (varies with programmable settings)
Frequency Synthesis	Fully digital (frequency switching time < 1 μs)
Pulse Repetition Rate	50, 100 and 200 pps
Pulse Width	33 to 533 μs for VIS waveform, 275 ms for OIS
Signal Processing	
Processors	Two Industrial x586's and Texas Instruments TMS320C40
Range Bins	Up to 512
Height Range	0-2560 km (0 km used for self-calibration)
Height Resolution	5 km (reciprocal of receiver bandwidth) 250 m using High Range Resolution measurement
Amplitude Resolution	3/8 dB
Phase Resolution	1.3°
Doppler Resolution	25 mHz (depends on integration time)

REFERENCES

Breit, G. and M.A. Tuve, (1926) A test for the existence of the conducting layer, *Phys. Rev.*, **28**, 554-575.

Haines, D.M. (1994) *"A Portable Ionosonde Using Coherent Spread Spectrum Waveforms for Remote Sensing of the Ionosphere"*, Thesis UMASS Lowell.

Huang, X. and B.W Reinisch (1996) Vertical electron density profiles from the Digisonde network, *Adv. Space Res*, **18**, 6, 121-129.

Reinisch, B.W. (1996) Modern Ionosondes, in *Modern Ionospheric Science*, (Editors H. Kohl, R. Rüster, and K. Schlegel), European Geophysical Society, 37191 Katlenburg-Lindau, ProduServ GmbH Verlagsserie, Berlin, Germany, 440-458.

Reinisch, B.W., D.M. Haines, K. Bibl, I. Galkin, X. Huang, D.F. Kitrosser, G.S. Sales, and J.L. Scali (1997) Ionospheric sounding support of OTH radar, *Radio Sci.*, **32**, 4, 1681-1694.

Scali, J. L., B. W. Reinisch, C. J. Heinselman, and T. W. Bullett (1995) "Coordinated Digisonde and incoherent scatter radar F region drift measurements at Sondre Stromfjord", *Radio Sci.*, **30**, 5, 1481-1498.

7. 30 MHz Riometer

Jens C. Ostergaard
NorthWest Research Associates

Introduction

The Riometer operates at 30 MHz; the standard frequency used world wide for monitoring of ionospheric absorption, enabling comparisons with other locations and previous, as well as future measurements. Ionospheric absorption is caused by solar radiation penetrating into the ionosphere's D-region at 40 - 90 km altitude and ionizing atoms and molecules in the atmosphere. The collision frequency in this part of the ionosphere is high, and the increased ionization causes absorption of radio waves passing through it. The absorption is a function of frequency and the path length within the absorbing medium. Lower frequencies are absorbed more than higher frequencies and the absorption increases with path length through the absorbing region.

Three different mechanisms account for D-layer ionization. Solar UV radiation enhances D-region ionization during daylight hours. This results in a low-level absorption of a few tenths of a dB at 30 MHz. Auroral electron precipitation creates patches of absorption in the auroral zone. The level of absorption as seen on a classic riometer ranges from a few tenths of a dB to 5 - 6 dB. The duration is relatively short, from minutes to hours. Finally, high energy, solar protons funneled into the Polar Cap Regions during large solar flares create high absorption, in the range from 1 dB to and sometimes exceeding 20 dB. Such absorption events occur most frequently around the maximum of the 11-year solar cycle, and they cover the Polar Cap region.

All three types of absorption events can be observed at the HAARP site, although no Solar Proton Events have been seen during the first years of operation, as this period includes the minimum solar activity in the last cycle. The maximum solar activity in the current solar cycle is expected in the years 1999 – 2001, and effects of Solar Proton Events may be seen during this period.

Measurement of Ionospheric Absorption at VHF

The riometer measurement technique is well known and documented in texts on radio astronomy, radiometry and ionospheric absorption measurement [1,2,3]. Riometry has evolved as a special case of space radiometry for direct measurement of the nondeviative absorption in the Earth's ionosphere. A riometer is a radio receiver with an antenna set up to measure the Galactic noise at zenith.

The riometer installation consists of a four-element array of crossed yagi antennas arranged in a square as shown in Figure 1. The main beam is pointed at zenith. The omnidirectional antenna radiation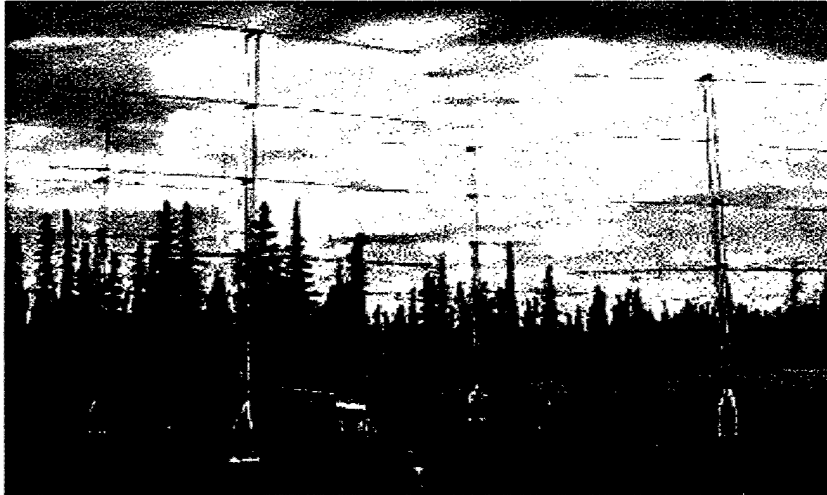 pattern is shown in Figure 2. The antenna array is coupled to a receiver capable of accurately measuring the noise power delivered by the antenna array. The measured noise power is recorded by a PC fitted with an A/D converter, data storage and analysis software. The antenna noise primarily originates from radio stars in the Galaxy, hence the name Galactic noise. When no

Figure 1. Riometer antenna array and receiver enclosure.

ionospheric absorption is present, the Galactic noise reaches the antenna without attenuation, but any absorption in the ionosphere's D- and E- region attenuates the Galactic noise. Figuratively, the lower ionosphere becomes opaque to the Galactic noise. Hence the name RIO-meter: Relative Ionospheric Opacity meter. The absorption can then be derived by comparing the signal from a time without absorption to the signal during an absorption event.

The galactic noise is time invariant with respect to celestial coordinates. However, as the Earth rotates, the galactic noise varies with time when observed from a point on the surface of the Earth. The diurnal variation is repetitive with respect to sidereal time but not with respect to solar time. Accumulated solar time and

Figure 2. Riometer antenna radiation pattern.

sidereal time differ by 24 hours a year, or four minutes a day. During undisturbed ionospheric conditions, the measured noise will follow a simple pattern repeating each 24 hours of sidereal time. This diurnal pattern is termed the QUIET DAY CURVE. The quiet day curve is displaced four minutes a day, relative to solar time. Slight, seasonal variations, presumably in the higher ionosphere, introduce a small variation of the quiet
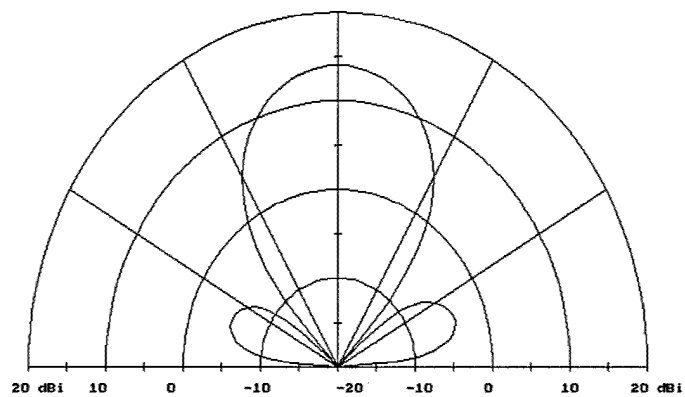
day curve over the year. Traditionally, riometer recordings were examined and scaled by hand. Such a procedure, although very accurate when done properly, is expensive and does not yield real time absorption figures. The HAARP riometer has the seasonally adjusted quiet day curves built into the data collection and analysis computer. This way, real time absorption data can be derived.

An example showing a four-day record of riometer measurements is given in Figure 3. The blue curve is the quiet day curve. The black dots are values of the received noise signal recorded once a minute. The red curve shows the one way
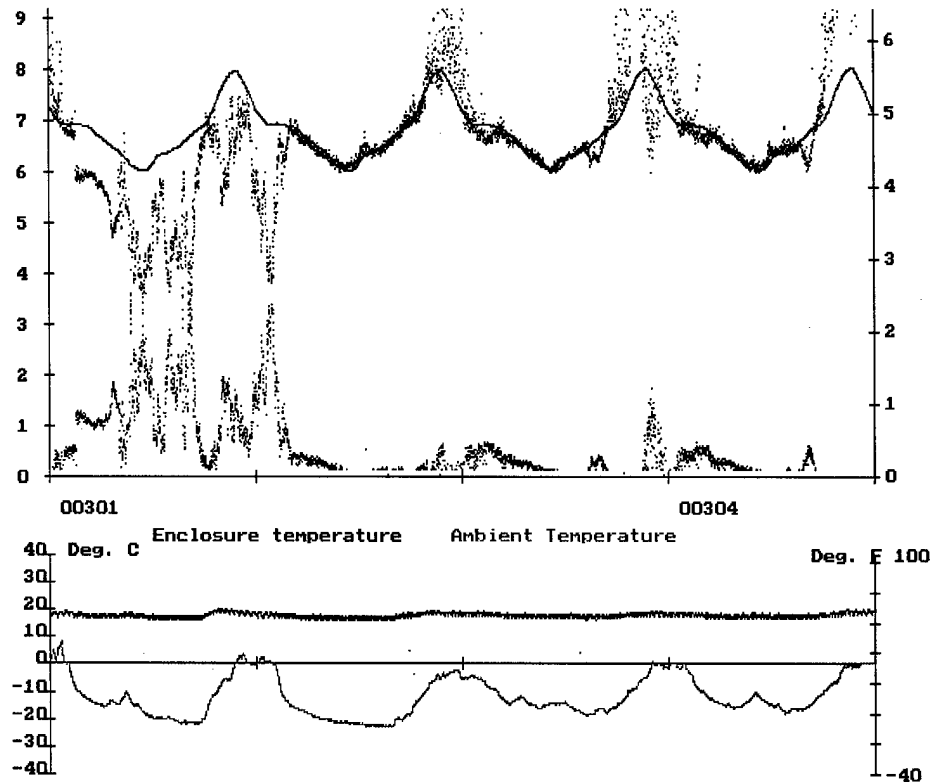

Figure3. Example of riometer data.

ionospheric absorption at zenith derived from the difference between the quiet day curve and the measured noise. The two curves at the bottom of the figure show the riometer receiver temperature (red) and the ambient temperature at the riometer site (green).

REFERENCES

1. Rawer, K. ed. (1976) *Manual of ionospheric Absorption Measurements*. U.S. Dept. of Commerce, NOAA, WDC A.

2. Hargreaves, J. K. (1969) Auroral Absorption of HF Radio waves in the ionosphere: A review of the first decade of riometry. *Proc. IEEE*, **57**, 8.

3. Ostergaard, J.C. (1995) *The HAARP 30 MHz riometer. The first years*. Boston College, Institute for Space Research.

8. Imaging Riometer

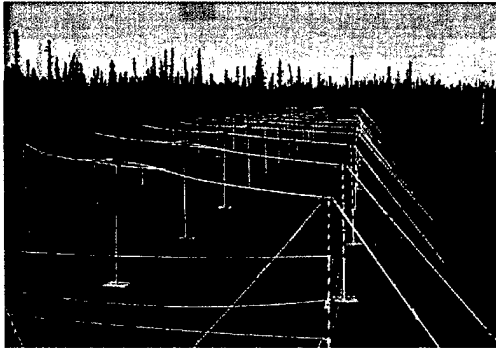T.J. Rosenberg, A.T. Weatherwax, D.L. Detrick, L. Lutz, J. Etter
University of Maryland

Figure 1. The prototype 16-beam, 38.6 MHz riometer.
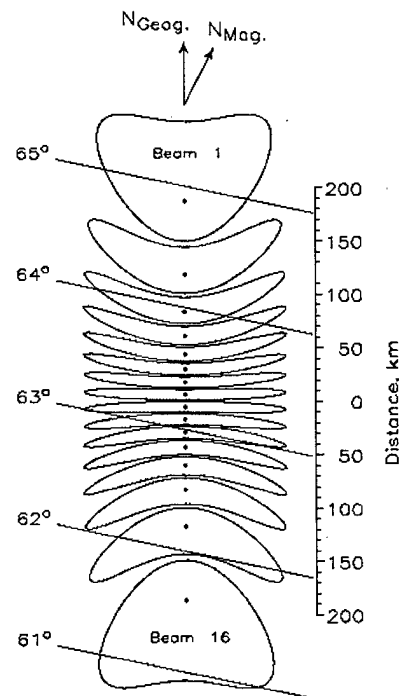
Riometer Basics

The riometer technique for examining electron density enhancements in the ionosphere is based on the absorption of cosmic radio noise, the broadband RF energy radiated by stellar sources in the galaxy. Riometer measurements are usually made at frequencies in the range of 20 to 50 MHz because the absorption of radio energy at these frequencies is sensitive to changes in electron density and collision frequency in the ionospheric D- and E-regions. Auroral absorption is most often caused by the precipitation of energetic (> 10 keV) electrons from the magnetosphere, which increases the ionospheric electron density between about 70 and 120 km altitude. The Imaging Riometer for Ionospheric Studies (IRIS) system [*Detrick and Rosenberg*, 1990] operates as a fast-scan multiple-beam instrument capable of examining the entire ionospheric sky, out to about 45° from the zenith, and examining ionospheric electron density perturbations in fine time scale, as well as small spatial scale.

The HAARP Imaging Riometer

The HAARP imaging riometer [*Rosenberg et al.*, 1999], as depicted in Figure 1, is capable of examining the heater perturbed region with sufficient spatial and temporal resolution to aid in characterizing the ionospheric parameters that are critical for understanding and controlling the conversion of HF heater power to other forms. The present instrument consists of a 1×16 antenna array phased in one dimension (beam width of 6.7°) and oriented approximately along the magnetic meridian. Figure 2 shows the projection onto the ionosphere at 90 km altitude of the antenna beam pattern (-3 dB contours)

HAARP Riometer Diagnostic
Ionospheric Projection, 90 km

Figure 2: Ionospheric projection of the prototype 16 element HAARP riometer . The antenna array is phased only in the geographical meridional direction, with the 16 beams numbered 1 (most northern) through 16 (most southern). Lines of constant magnetic invariant latitude 61° to 65° are indicated. The point of maximum sensitivity for each beam is indicated by the black dot.

and the orientation of the beams with respect to the north geographic and geomagnetic poles. This prototype system is the forerunner for a full-scale imaging riometer that would consist of a 256-element antenna array (16×16).

Data Presentation Example

In addition to operating during low-power transmissions, the riometer has provided high-quality data on naturally-occurring auroral activity, including some surprising observations. The imaging riometer responds sensitively to natural variations of auroral absorption, such as those caused by magnetospheric substorms, and provides clear evidence of its capability to discern spatial structure and motion. In fact, a newly observed feature has been documented near dusk using the HAARP imager. These intense, short-duration absorption spikes are accompanied by only weak magnetic signatures, and the spatial and temporal morphology of these spikes, and their relationship to substorm processes, are subjects of current study. An example of such an event in riogram format is shown in Figure 3. The riogram is analogous to an optical keogram, where a meridional slice through an all-sky camera is displayed. In Figure 3, the ordinate is depicted as distance at a 90 km altitude range (D-region) with north (south) at the top (bottom) and UT time is along the abscissa.
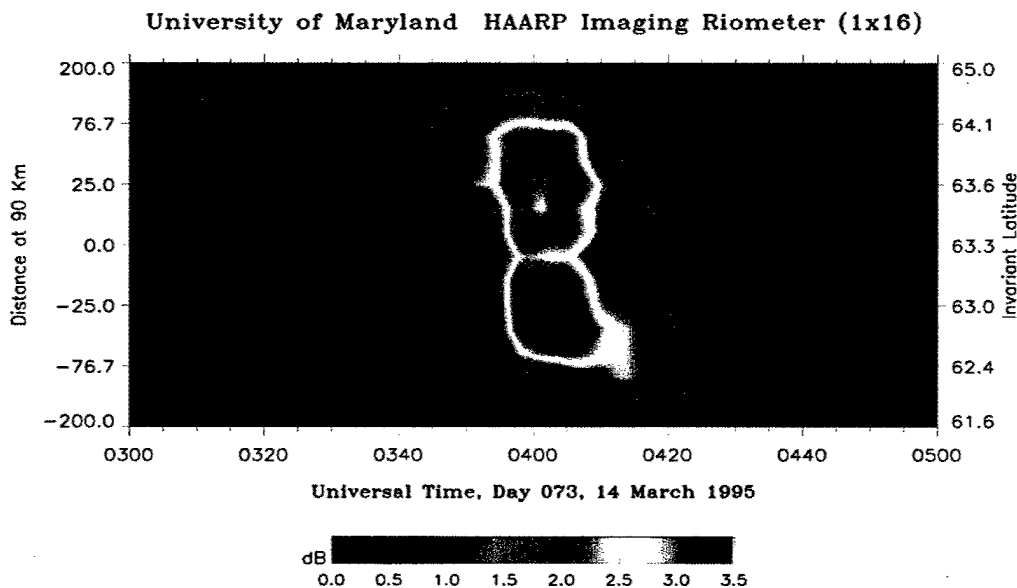
Figure 3. A keogram-style display of the latitude-time-intensity variations of absorption. The display ranges from north (beam 1) at the top to south (beam 16) at the bottom. Note the nonlinearity of the ordinate scale, which reflects the projection of the maximum sensitivity point of each beam (see Figure 2). The level of absorption in dB is given by the color bar. The spatially localized and broad absorption spikes near dusk (0400 UT) are evident. Note that the sharp spike at 0310 UT is confined to the northern half of the array and that both spikes exhibit equatorward drift.

44

Computational Efforts

Using a 1-D numerical code that solves simultaneous equations for electron energy balance and wave propagation we compute maximum changes of ν_e (electron-neutral collision frequency) and T_e (electron temperature) for continuous periods of ionospheric heating from which changes in N_e (electron density) can be found. Absorption estimates before heater turn-on using ambient ν_e, T_e, and N_e values are compared with absorption estimates using estimated heater-modified values of these quantities. Calculated riometer absorption (Fig. 4) suggests marginal detectability of heater-induced effects for the 960 kW configuration used in the spring 1999 campaign. Analysis of the campaign data is in progress. No evidence of heater-induced effects is thus far apparent. Later campaigns will have higher powers available, increasing the likelihood of observing absorption.
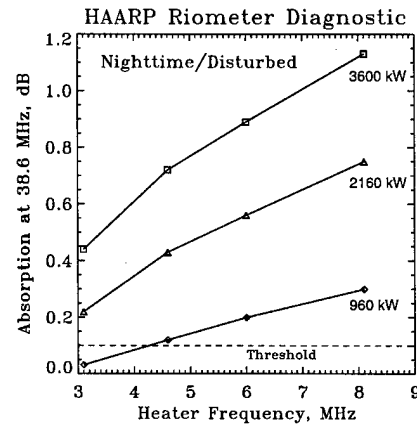
Figure 4. Predicted riometer absorption at zenith for night-time/disturbed, ionospheric conditions. The detection threshold assumes uniform widespread absorption over the

REFERENCES

1. Detrick, D.L., and T.J. Rosenberg (1990)A phased-array radiowave imager for studies of cosmic noise absorption, *Radio Sci.*, **25**, 325.
2. Rosenberg, T.J., A.T. Weatherwax, D.L. Detrick and L. Lutz (1999) High Frequency Active Auroral Research Program imaging riometer diagnostic, *Radio Sci.*

8. MHz Coherent Backscatter Radar

Frank Djuth[1] and Keith Groves[2]
[1]Geospace Research
[2]Air Force Research Laboratory

The HAARP VHF radar nominally operates at a frequency near 139.3 MHz. At this frequency external interference is minimal and the transmitters are well matched to the antenna array. The overall system design is robust enough to accommodate frequency changes within an 8 MHz bandwidth (135 MHz - 143 MHz). The basic radar architecture has four key elements: a planar phased-array antenna, sixteen distributed solid state transmitters, a four-channel Digital Down Converter (DDC) receiver, and a real-time radar processor system. The antenna consists of a 32 × 24 array of collinear, coaxial dipoles (CoCos). It is divided into four sub-arrays having eight lines of 24 dipoles each (quads). One solid-state transmitter having ~2.0 kW peak power is divided among two CoCos. Figure 1 shows the antenna array along with two trailers to the right used to house the radar. The small trailer isolates the sensitive radar receiver front end from the transmitter and digital electronics in the main radar trailer. A small plasma line array in the foreground of Figure 1 was used to detect the HF-enhanced plasma line during an experiment conducted in August 2002.
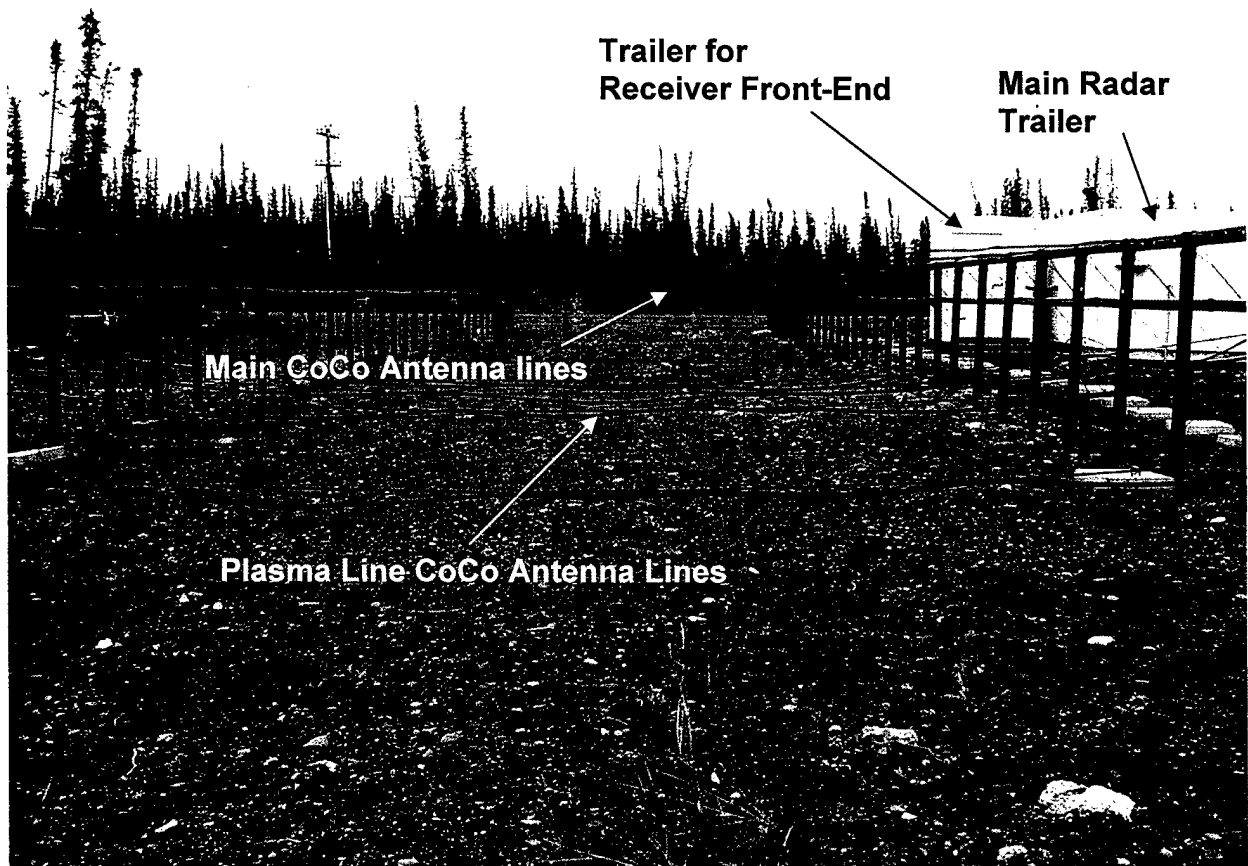

Figure 1. HAARP VHF antenna array and trailer enclosures that house the radar.

47

A block diagram of the 139 MHz radar architecture is provided in Figure 2 below. The key components are: the local oscillator (LO) box, two transmitter (TX) units, sixteen power amplifiers (PA), four transmit-receive switches (T/R), a four-channel analog down-converting receiver (REC), a four-channel IF interface unit (IFMPX), a digital control interface box (CI), a digital transceiver, and thirty-two collinear-coaxial (CoCo) antenna lines. An external 10 MHz overnized crystal usually serves as the system reference oscillator. This oscillator is power-divided through a distribution-amplifier having 7 isolated ports. The outputs of the distribution amplifier are directed to the LO box, the CI, and user-supplied diagnostic equipment used to monitor system performance. Alternatively, there is an internal 10 MHz oscillator within the LO box that has an output bnc connection for routing to the 10-MHz distribution amplifier. The selected 10 MHz reference is used by the LO box to phase lock a 129 MHz Phase Locked Loop (PLL) signal source. The LO box accepts control signals from the CI (via a DB25 ribbon connector) and translates them into TTL signals with the aid of a Control Circuit Board (CCB).

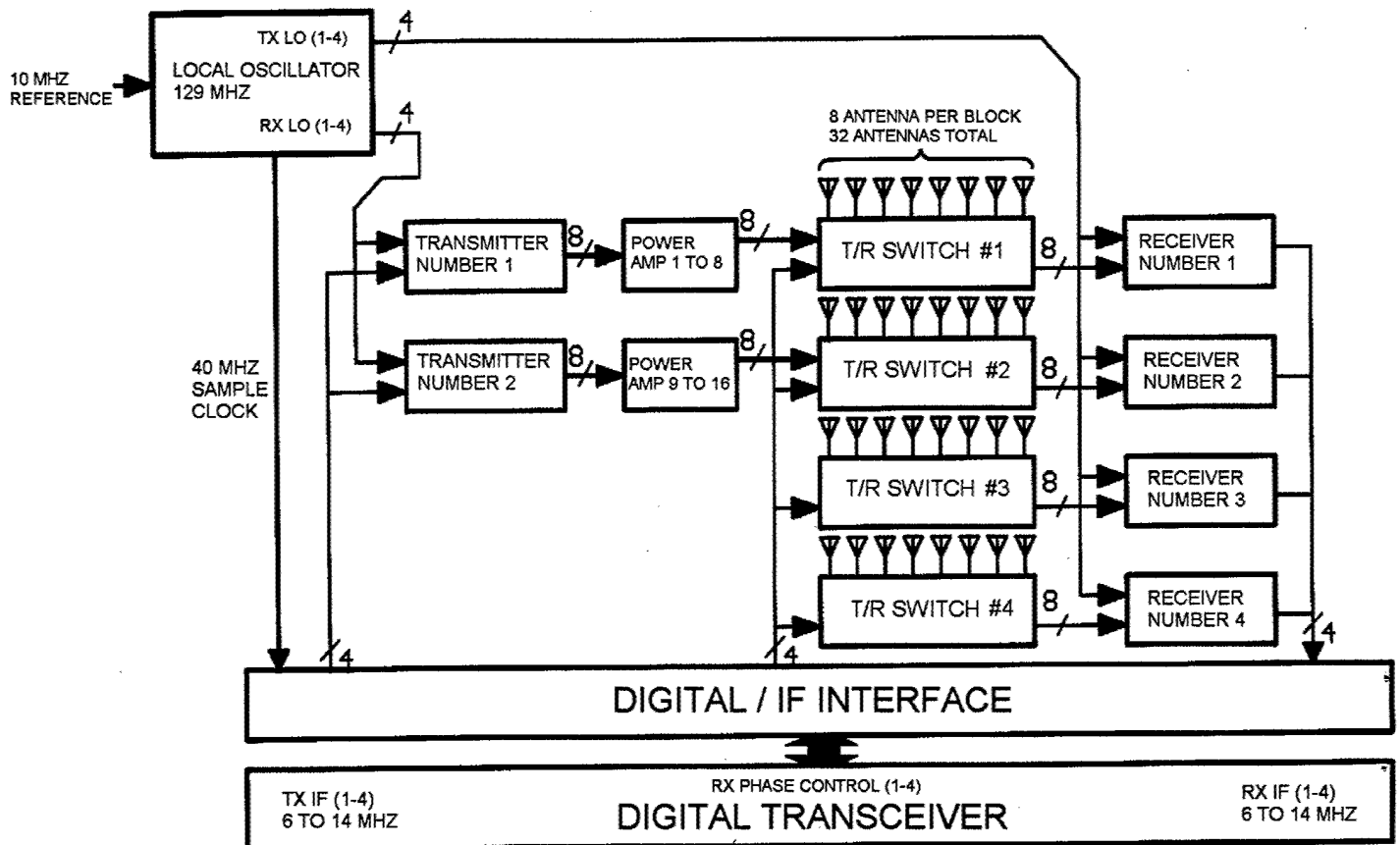*Figure 2. Block diagram of the VHF radar architecture showing the principal components.*

The role of the transmitter box is to generate eight 5-W phase-locked pulse outputs that can be used to drive the power amplifiers. The unit mixes the 129 MHz TX pulse from the LO box with a 6-14 MHz pulse from the IFMPX to form a pulse at the right frequency and phase for the power amplifiers. The frequency and phase of the TX

IF input is set by a synthesizer that is controlled across the VME bus. Thus the actual radar frequency transmitted in the band 135 MHz to 143 MHz and the transmitter signal phase are under computer control.

The seed pulse from the transmitter unit is power divided into three signals. Each signal is subsequently amplified to approximately 30 W prior to entering one of three solid-state power modules. The phase of the power module output signals are adjusted so that all three amplified signals have the same phase. These signals are subsequently power combined to yield radar pulses that have a power of $\geq$ 2 kW. The DC power supplies used for the three solid state power modules operate at ~37-38 V and produce current levels $\geq$ 70 amp.

The output of each power amplifier is inserted into a circulator, which is the first component of the T/R switch. The circulator provides a stable 50 ohm load for the power amplifiers and a means of depositing reflected power in a load. This prevents reflected power from propagating to the output terminal of the power amplifier. The specific concern is not the reflected power experienced during normal radar operations. This is relatively small because VSWRs range from 1.2:1 to 1.3:1. However, in the event that the antenna were damaged by wildlife during unattended radar operations, the VSWR could reach high enough values to destroy some of the power amplifiers. A load bank prevents this from happening. In the current configuration, the outputs from eight circulators are power-combined before entering the T/R switch. This is done to reduce signal losses to and from the antenna. A low loss transmission line (Andrew Corp. Heliax, LDF450A, 0.7 dB/100 ft at 139 MHz) connects the transmit port of the T/R switch to each eight-way power divider in the antenna array. The power is then distributed equally to eight CoCo antenna lines. The receiver port of the T/R switch is connected to a low noise preamplifier, the output of which serves as the input for the down-converting analog receiver. The TTL control for the T/R switch originates in the CI, and is sent across the data bus to a CCB in the LO box which relays the bus information to a T/R CCB.

The digital radar subsystem generates the IF radar waveform, controls radar timing, monitors radar status, and receives and processes the received IF signal. A block diagram of this system is provided in Figure 3. It consists of 12 main components: 1) console, 2) data processing unit (DPU), 3) data input/output (I/O) capability, 4) electronic timing and control (ETAC), 5) digital input/output (DIO), 6) analog to digital conversion (ADC), 7) wideband (WBRX) and narrowband (NBRX) digital receivers, 8) direct digital synthesizer (DDS), 9) control interface (CI), 10) Failsafe Pulse Screen (FPS), 11) IF multiplexer (IFMPX), and 12) analysis system. Seven of these components are housed within a VME bus rack (ETAC, DIO, ADC, WBRX/NBRX, DDS, DPU, and DSP). The CI and Failsafe systems reside in the same enclosure and are connected to the VME system via several high-density cables.

The system specification for the VHF radar is provided in Table 1 below. An important guideline for operating this radar entails the maintenance of an ambient temperature between 0 C and 40 C. Even in storage the system should be kept within this temperature range to prevent damage to the many electrolytic capacitors and other temperature-sensitive components in the system. Although the transmitter and receiver can be tuned between 135 MHz and 143 MHz, there are limitations on what can be

radiated by the existing CoCo antenna. A CoCo antenna exhibits a linear response to input signals, so it will radiate at any frequency. However, phase errors will develop across the antenna array giving rise to a broadened beam. The matching network at each CoCo antenna ultimately limits the radar transmission bandwidth. The effective bandwidth of the matching network is approximately 2 MHz and extends from 138.5 MHz to 140.5 MHz.
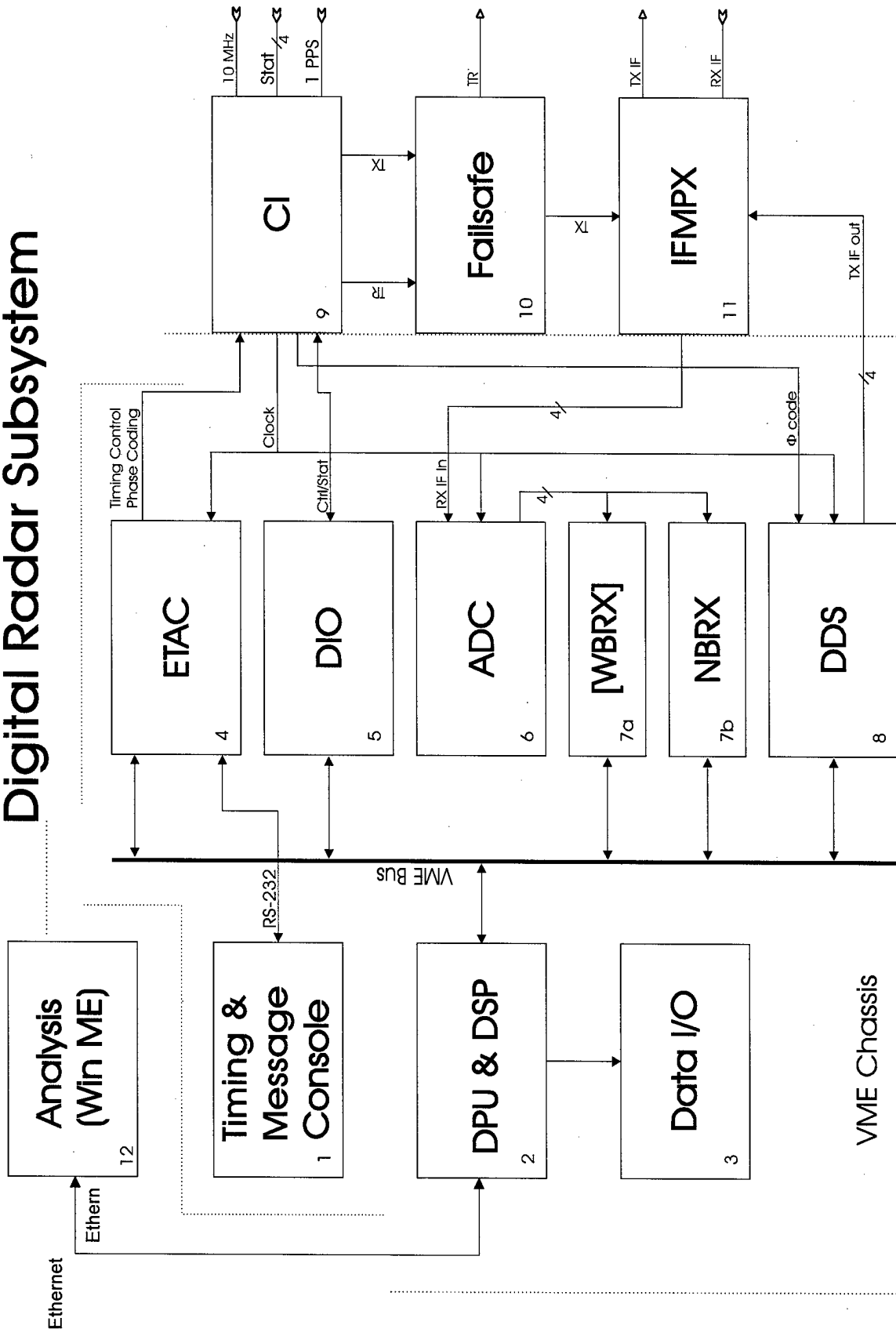
Digital Radar Subsystem

Figure 3. Block diagram of the digital radar subsystem showing major components.

51

Table 1. VHF Radar Specifications

SYSTEM	
Operating Temperature	0-40 C
Power Requirement	220V, 50-60 Hz, 4 kW
Power Requirements	110V, 50-60 Hz, (6 + 3) kW
TRANSMITTER	
Center Frequency Range	135 MHz - 143 MHz
Instantaneous Bandwidth	$\geq$ 2 MHz
Configuration	16 distributed solid-state amplifiers
Peak Power Per Power Amplifier	2.0 kW nominal
Total Peak Power	32-40 kW nominal
Maximum Duty Cycle	10%
Maximum Pulse Width	2 ms
Minimum Pulse Width	0.5 μs
Pulse Coding	180°, coding sequence is digitally controlled, minimum baud length is 1μs
Phase Control	Four quadrants, each consisting of four 2.0-kW transmitter modules, are phased under computer control
ANTENNA	
Collinear, Coaxial, Dipole Rows With Phase Steering of Beam	32 Rows, 24 dipoles each, one-way gain for entire antenna ~34 dBi, ERP~70 MW (with losses), antenna bandwidth ~ 2 MHz
T/R SWITCH (Circulator + Limiter + GaAs FET Switch)	
Transmitter Port VSWR	< 1.7
Loss - TX Port to Antenna Port	< 1.0 dB
Loss - Antenna Port to RX Port	< 1.0 dB
Control	Digital
SYSTEM PROTECTION	
Duty Cycle, RF Pulse Width, T/R Logic	Autonomous checking every IPP
Power Supply Voltages for Amplifiers	Automatically checked by autonomous system
RECEIVER	
Configuration	Analog circuitry to 10 MHz (+6/-8 MHz) IF, Digital downconversion and decoding thereafter
Receiver Frequency Range	131 MHz - 145 MHz
Number of Analog Phase Shifters	4
Number of Analog Front-end Channels	4
Number of Complex Digital Receiver Inputs and Complex Digital Channels	Digital wideband receiver (625 kHz -20 MHz), 4 inputs and 4 channels Digital narrowband receiver (305 Hz - 625 kHz), 4 inputs and 8 channels
Reconfiguration Time for Filter Bandwidth and Tuned Frequency	One interpulse period
A/D Converter	Four Channels, 12-bits, 40 megasamples per second each
Noise Figure	< 0.5 dB
Timing Reference	10 MHz internal or external
Internal Reference Stability	10^{-10}
Internal Reference Phase Noise	< -130 dBc/Hz at 10 Hz offset

To date, the HAARP VHF radar has been used in studies involving polar mesospheric summer echoes (PMSE), meteor plasmas, the detection of HF-enhanced plasma lines, and other interesting echoes of unknown origin. An example of PMSE echoes recorded during the summer of 2002 is provided in Figure 4 below. A 13-baud Barker coded pulse with a 20 μs baud length and a 10 ms IPP was used for these measurements. The strongest echoes were detected during a 1.7 hour period beginning just before 21:00 Alaska daylight time (ADT); weaker echoes were observed throughout a three hour period. The spectral width is proportional to the mesospheric wind speed at the PMSE altitude, and structure within the PMSE spectra is indicative of spatial inhomogeneities within the layer.
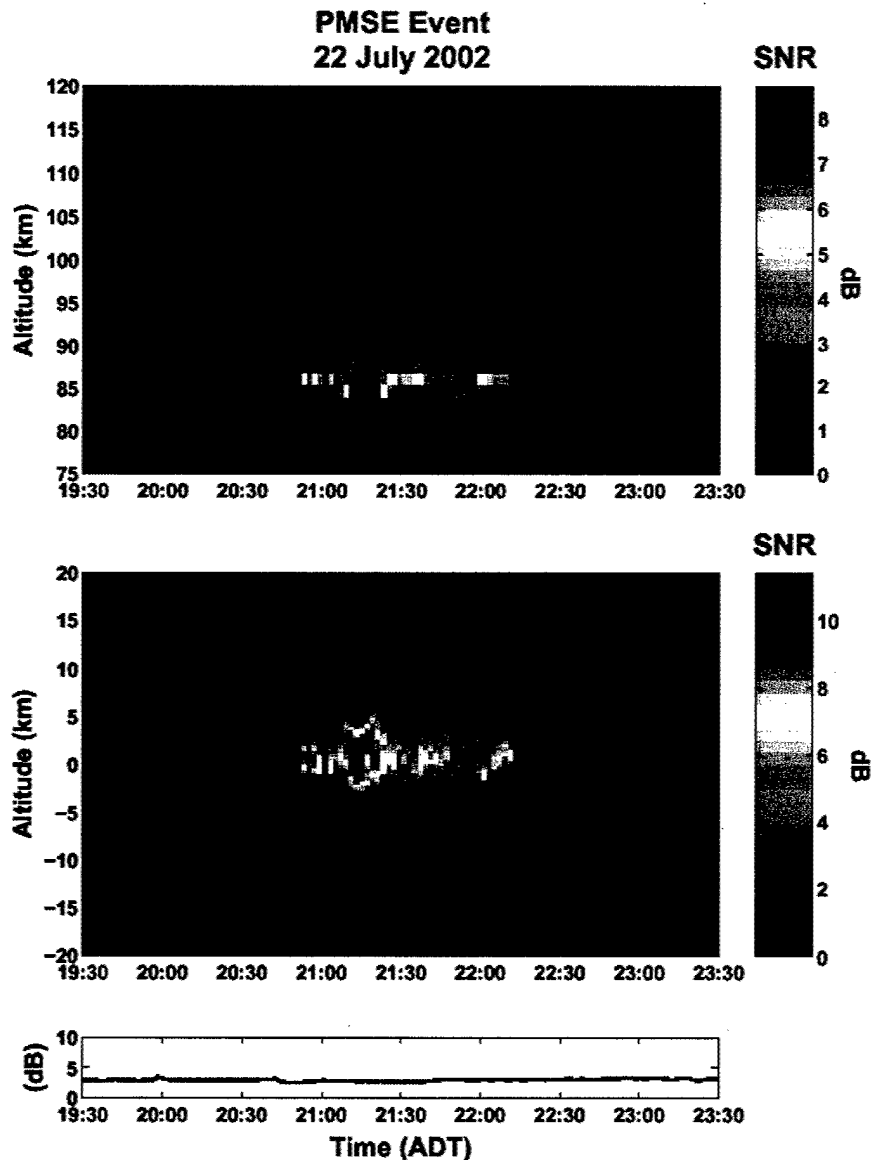

Figure 4. Range-time-intensity plot of a segment of PMSE data (top panel) and the same PMSE observations shown in the spectral domain (middle panel). Frequency is referenced to the radar operating frequency (139.3 MHz). The bottom panel shows the background noise level relative to the lowest noise level achievable at HAARP.

9. Relative TEC - Latitudinal Scans

Ed Fremouw
NorthWest Research Associates

Introduction

The line integral of plasma density through the ionosphere is referred to as "total electron content" (TEC). At VHF and above, where departure of the radio refractive index from unity is closely proportional to plasma density and where bulk refraction may reasonably be ignored, one may exploit the dispersive nature of radio wave propagation in a plasma to measure TEC. The technique requires transmission and reception of two or more mutually coherent signals over a transionospheric path. Six Oscar-class Transit satellites of the Navy's Ionospheric Measuring System transmit coherent pairs near 150 and 400 MHz from high-inclination circular orbits near 1000 km altitude, as do several Russian satellites and others either launched or planned by DoD, such as RadCal, ARGOS, and DMSP S15 (some of which orbit near 800 km altitude).

Measurement Approach

NorthWest Research Associates (NWRA) developed a coherent radio receiving system (the ITS10) specifically for measuring, at one sample per sec (sps), dispersive phase between the two phase-coherent signals received from a Transit satellite. Using simple dipole antennas over a ground screen, the receiver locks to the UHF signal when a Transit rises above the horizon. It then continuously measures the dispersive phase between that reference and the Transit's VHF

Figure 1. ITS10S VHF (against sky) and UHF (lower) dipoles over ground screen.

signal until the satellite sets, producing a latitudinal scan of "relative" TEC across Alaska. In a later augmentation, the ITS10 was modified to measure the intensity of the two signals as well as the dispersive phase between them, each at 50 sps. The augmented receiver is known as the NWRA ITS10S (S for "scintillation"), which now is installed and operating in the optics shelter at Gakona. Figure 1 shows the antennas and their ground screen, in front of the shelter.

The ITS10S receiver outputs the VHF quadrature components (I and Q), using UHF as a phase reference, and the UHF I (= amplitude, since its Q and phase are zero by virtue of signal lock). The I and Q values are recorded at 50 sps in ASCII files named

55

'date_time.its' (where 'date_time' identifies the date and time of satellite rise) on the disk of an associated PC. The values also are converted to intensity, $I^2 + Q^2$, and dispersive phase, $\delta\phi$, for real-time display on the PC's monitor during the pass. Immediately following a pass, the PC converts $\delta\phi$ to relative TEC, smooths the values to one sps*, and computes relevant geometrical information. The results are stored in ASCII files called 'date_time.pro' (for "processed").

Subject to the 2nπ ambiguity indicated below, $\delta\phi$ is related to T, the "absolute" TEC as follows:

$$\delta\phi + 2n\pi = r_e \lambda_V (1 - m^2) T$$

where r_e is the classical electron radius, λ_V is the VHF wavelength, and m (= 3/8) is the ratio of the UHF to VHF wavelengths. In processing, we absorb the ambiguity into an unknown bias in T by subtracting the minimum value of dispersive phase recorded during the pass (usually near the point of closest approach, where the transionospheric pathlength is shortest), as follows:

$$\Delta\phi = (\delta\phi + 2n\pi) - (\delta\phi + 2n\pi)_{min} .$$

Thus, with $\Delta\phi$ in radians, we obtain relative TEC in units of 10^{16} el/m², as follows:

$$T_r = [10^{16} r_e \lambda_V (1 - m^2)]^{-1} \Delta\phi = 0.0207 \, \Delta\phi$$

Data

The relative TEC data and attendant path-geometry information, along with data-quality flags, are available on the HAARP Diagnostic Server in netCDF files called 'date_time.nc', as are the 'date_time.pro' ASCII files. Both the files and graphical presentations of the data are available in the Relative TEC Archive accessible from the Data Index page on the HAARP website. A graphical example follows.
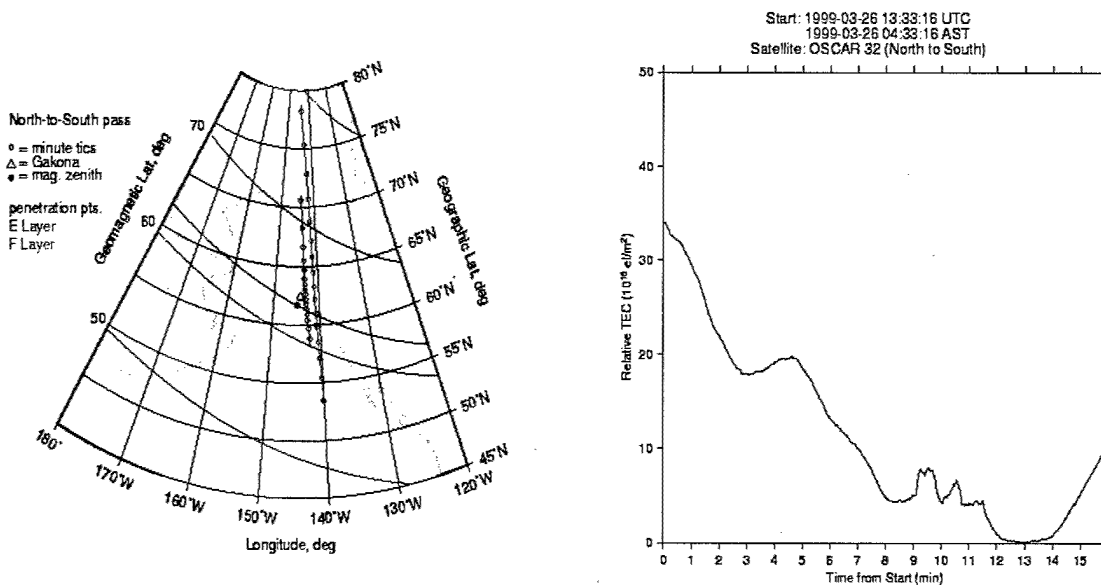

56

10. Absolute TEC from GPS

Ed Fremouw
NorthWest Research Associates

TEC Basics

The line integral of plasma density through the ionosphere is referred to as "total electron content" (TEC). At VHF and above, where departure of the radio refractive index from unity is closely proportional to plasma density and where bulk refraction may reasonably be ignored, one may exploit the dispersive nature of radiowave propagation in a plasma to measure TEC. The technique requires transmission and reception of signals at two or more sufficiently separated frequencies over a transionospheric path.
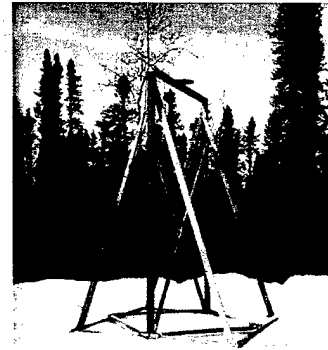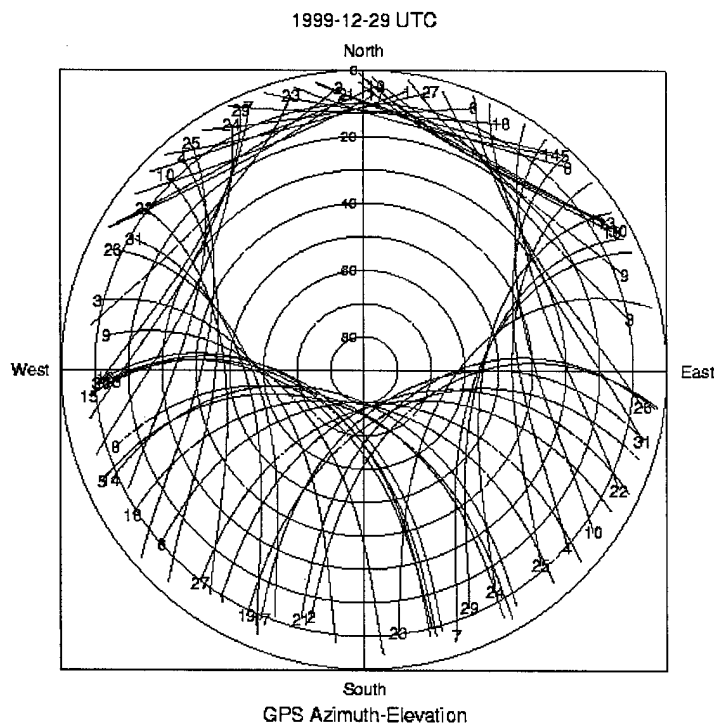
GPS antenna and equipment shelter

Measurement Technique

All satellites of the Global Positioning System (GPS) transmit on two L-band frequencies, referred to as L1 (1575.4 MHz) and L2 (1227.6 MHz). Given an appropriate GPS receiver, one may obtain an unambiguous (albeit somewhat noisy) estimate of absolute TEC by measuring the differential group delay (DGD) between the two frequencies as a particular satellite moves slowly across the sky. Figure 1 shows the GPS sky coverage at Gakona over a 24-hour period. (The

1999-12-29 UTC

GPS Azimuth-Elevation

Figure 1. Sky coverage (azimuth & elevation) of GPS satellites viewed from Gakona during a 24-hour period.

57

inclination of the GPS satellites precludes observation directly overhead and immediately north of the station.) One also may employ the differential (dispersive) carrier phase (DCP) between the two signals to obtain a highly precise (but ambiguous) measurement of relative TEC. An Ashtech Z-FX Continuously Operating Reference Station (CORS) is operated at Gakona for measurement of DCP and DGD. The combined measurements yield a smooth and unambiguous record of absolute TEC.

Subject to the $2n\pi$ ambiguity indicated below, the DCP, $\delta\phi$, is related to T, the "absolute" TEC as follows:

$$\delta\phi + 2n\pi = r_e \lambda_2 (1 - m^2) T,$$

where r_e is the classical electron radius, λ_2 is the L2 wavelength, and m ($= 120/154$) is the ratio of the L1 to L2 wavelengths. While (anomalous) dispersion in a plasma advances carrier phase relative to free space, group packets are retarded. The retardation increases with decreasing frequency, with the result that the DGD, Δt, is related to (absolute) TEC, T, as follows:

$$\Delta t = (r_e / 2\pi c) \lambda_2^2 (1 - m^2) T$$

where c is the speed of light in free space.

Instrument noise and differential group delays internal to GPS transmitters and receivers result in a measurement uncertainty such that, with Δt in nsec, the absolute TEC in units of 10^{16} el/m^2 recovered from DGD measurements is as follows:

$$T_a = [10^{16} (r_e / 2\pi c) \lambda_2^2 (1 - m^2)]^{-1} \Delta t = 2.85 \Delta t \pm \Delta T.$$

The noise contribution to ΔT can be diminished greatly by performing a least-squares fit between DGD and DCP measurements over a substantial portion of the several hours that a particular GPS satellite may be observed at a specific receiver location. (This process often is referred to as "phase-smoothing" the DGD record; it may equally well be viewed as "resolving the ambiguity" in the DCP record.) Substantial effort also has gone into evaluating the biases arising from individual transmitters, receivers, and pairs thereof, resulting in residual ΔT values of a few TEC units ($\sim$ a nsec uncertainty in Δt).

Absolute TEC data and attendant path-geometry information are available on the HAARP diagnostic server in netCDF files. Both the files and graphical presentations of the data are available in the Absolute TEC Archive accessible from the Data page on the HAARP website. An example for a single GPS pass is shown in Figure 2.
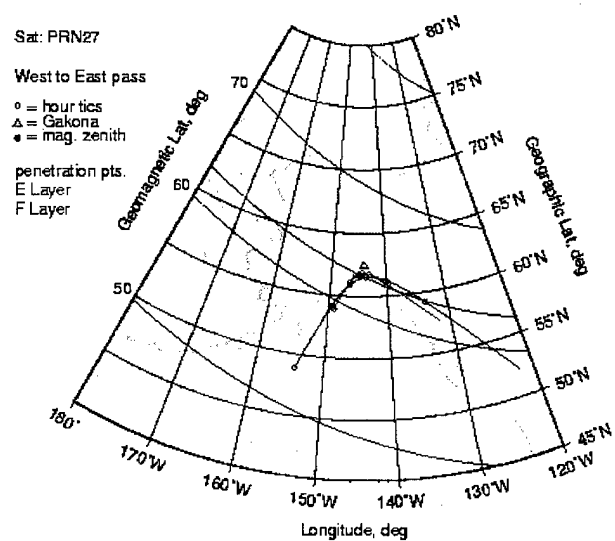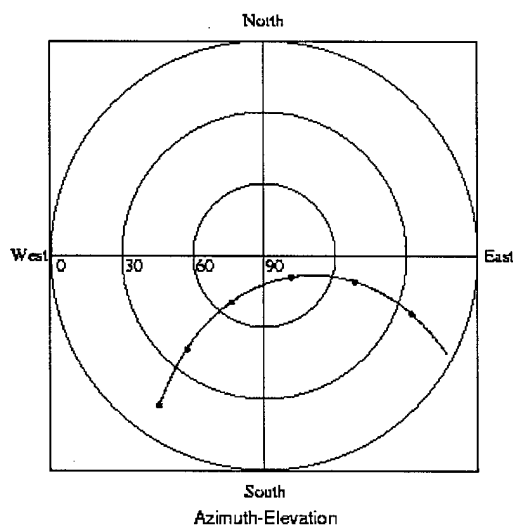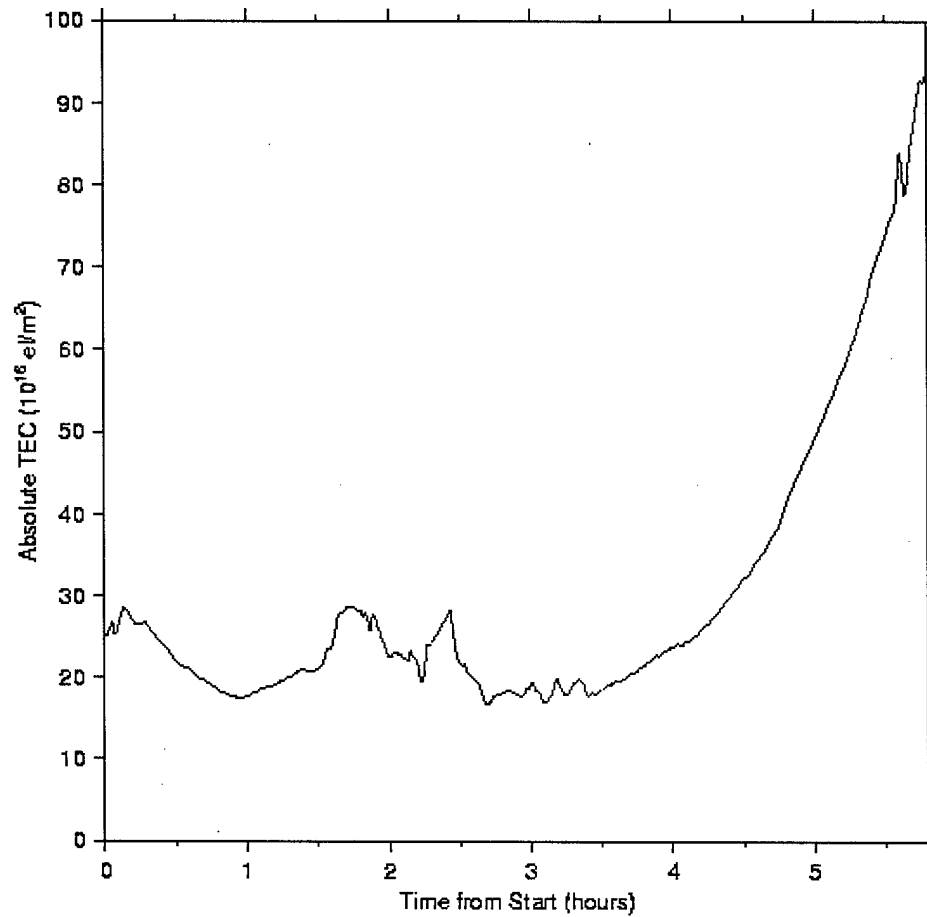
Figure 2. Absolute slant TEC (top) measured during GPS pass (bottom) from west to east just south of Gakona.

"Slant-path" TEC records such as that shown in the top panel of Figure 2 may be converted to "slab-equivalent vertical" TEC by multiplying the measured values by the secant of the zenith angle at the ionospheric penetration point (IPP) of the instantaneous ray path. (Such conversion treats the ionosphere as a horizontal slab collapsed to the altitude assumed for the IPP and, hence, does not account for plasma-density gradients.) Such a conversion is made for GPS data collected at Gakona on ray paths having elevation angles of at least 45 deg, using an IPP altitude of 350 km. As illustrated in Figure 3, results are posted on the HAARP web site as time series of local TEC displayed as a function of local time at the IPP (illustrated) or UTC (the default, for ease of comparison with other data). The data shown here include a period of early-morning ionospheric disturbance between two periods of somewhat lower than normal daytime TEC with quiet evening decays.
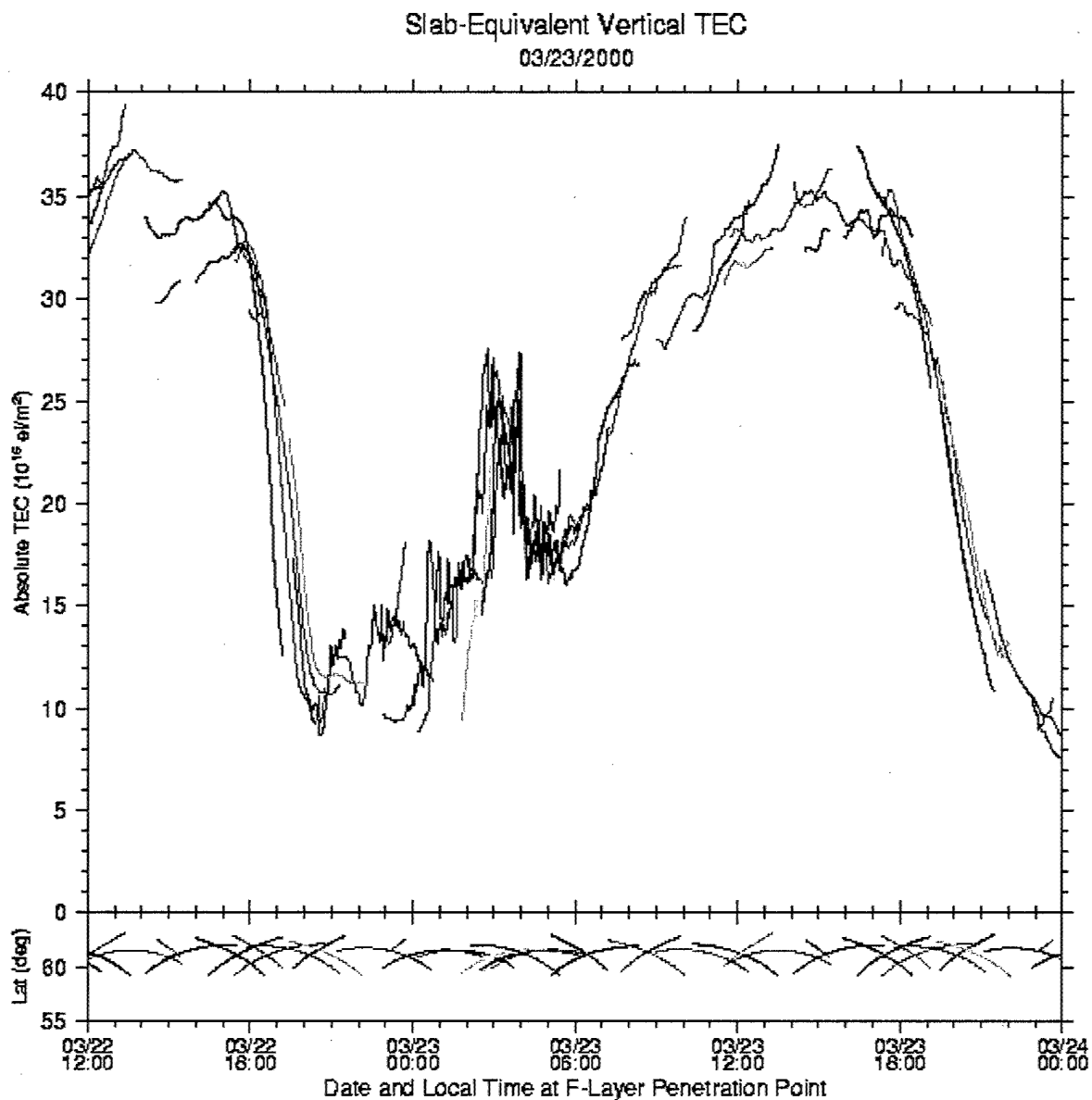

Figure 3. Time series of vertical TEC near Gakona. Span of geographic latitude covered is shown at bottom.

60

11. VHF Satellite Scintillation System

Bob Livingston
Scion Associates

Introduction

The HAARP VHF Diagnostic Satellite Scintillation (SATSIN) System is used to characterize the structure and dynamics of plasma irregularities in the ionosphere (the ionized portion of the atmosphere between 100 km and 1000 km). Such irregularities are a near-constant feature of the natural auroral zone, but can also be created by energy transmitted from the high-power HAARP array. Irregularities are produced by HAARP when its high-frequency radio energy is converted to heat in the ionosphere; the heating, in turn, weakly perturbs the background ionospheric plasma. This heating process (referred to as thermal self-focusing) occurs only over a small area over the antenna, and over a narrow range of heights. The specific altitude at which the heating occurs is between about 150 km and 300 km, and depends upon the state of the background ionosphere and the frequency transmitted from HAARP.

The SATSIN system characterizes plasma irregularities by the effect they have on a radio signal. The system receives VHF radio transmissions from a high satellite beacon; from the SATSIN site near Slana, Alaska, the radio path from the beacon passes directly over HAARP and through the ionospheric volume that is being heated. The heater-produced plasma irregularities perturb the radio signal slightly as it passes through, and SATSIN measures these "scintillation" effects.
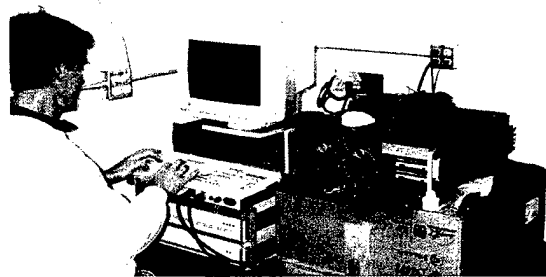

Figure 1. Data system.

Instrumentation

The system hardware consists of a high-performance eight-channel antenna/receiver system and two networked computers shown in Figure 1. The eight receiver antennas, one of which is shown in Figure 2, are distributed in an array over an area about 500 feet by 1000 feet in order to measure small spatial changes in the received signal. The amplified signals are sent from each antenna to the receiver that is located near the center of the antenna array. One of the system computers manages the receiver: optimizing signal levels and tuning, performing periodic diagnostic tests, and collecting data. It also processes the collected data to make it ready for analysis and transfers those data to the second

Figure 2. Helix antenna.

computer over a local network. The second computer performs the major numerical tasks: determining the time behavior of the scintillation data and analyzing the differences among the eight different receiver channels. It also acts as a network server so that the system data and system operations can be viewed in real time at the HAARP Diagnostics Center.

Data

The scientific parameters derived from the SATSIN system provide an accurate and extensive characterization of the plasma irregularities created by the heating. The amount of signal perturbation observed (an example is shown in Figure 3) can be related to the strength of the irregularities. The frequency spectrum of the data time series (see the example in Figure 4) indicates the size of the irregularities, and how they evolve in time. Perhaps the most important scientific capability of SATSIN comes from its multiple antenna configuration. Using correlation analysis of the signals received over the antenna array, the shape and movement of the irregularities generated by HAARP can be implied. These parameters are essential to an understanding of the physics of the thermal self-focusing process.

Figure 3. Time series of intensity and phase
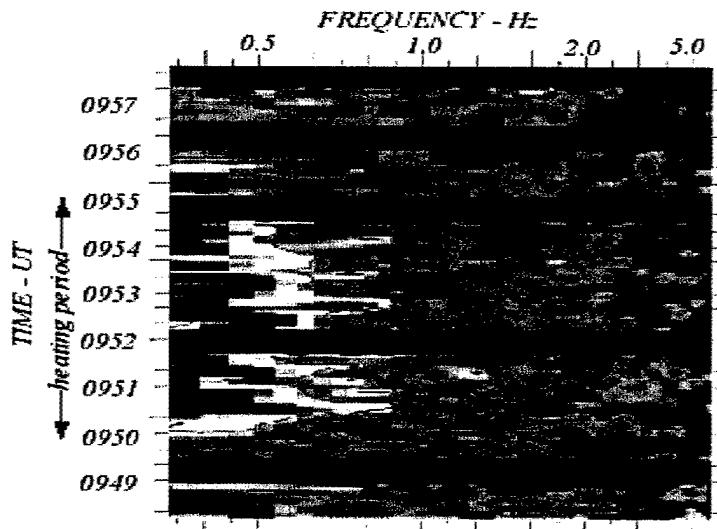
Figure 4. Frequency Spectrum of the time series

SATSIN collects data whenever there is a useful satellite signal (about 12 hours per day). Since the HAARP transmitter operates only infrequently, most of the SATSIN observations are of the natural background ionosphere. Many complex forces act upon the auroral ionosphere and lead to the formation of plasma irregularities. The completeness of the SATSIN observations provides a unique opportunity to gain insight into how these processes generate, transport, and remove irregularities. This is a key element in the overall HAARP diagnostic goal to obtain a detailed characterization of the ionosphere using data from multiple radio and optical instruments.
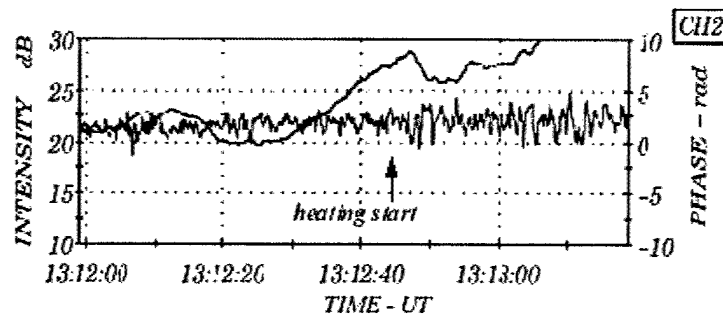
62

12. Modular UHF Ionospheric Radar

Brenton Watkins
Geophysical Institute, University of Alaska

One of the most useful diagnostic instruments available to the active ionospheric interactions research and applications community is a large power aperture, sensitive radar. This diagnostic technique relies on the scattering of radar signals by minute density irregularities and the random thermal ion and electron motions in the ionospheric plasma. This occurs even though a microwave radar frequency is used that is classically considered a line-of-sight signal unaffected by the ionosphere. However, a small fraction of the radar energy is reflected back. The returned signal characteristics can be analyzed to derive many important physical parameters, including electron density, electron and ion temperatures, electron and ion velocities, ion-neutral collision frequency, neutral wind, ionosphere conductivity, and current density.

The experimental determination of these physical parameters is vital to couple theory with observation of ionospheric effects initiated with a powerful high frequency transmit array. HAARP is a flexible HF transmit facility to investigate potential applications. However, the measurement of these ionospheric parameters is critical to understanding fully the effectiveness of defense applications arising from a high frequency transmit array.

From the outset of the High Frequency Active Auroral Research Program, a powerful diagnostic radar was identified as an essential diagnostic instrument. A series of panels, composed of users and radar experts, have defined the requirements for the HAARP diagnostic radar and have considered the various radar approaches. Table 1 summarizes the radar requirements.

Characteristic, Units	Value
Sensitivity, MWm^2/K	≥ 30
Beam Motion, deg/sec	≥ 1 over the portion of the hemisphere above 8° elevation or as above but also providing ≥ 100 over a 30° cone angle from the mechanical axis
Beamwidth, deg	Two-way, -6 dB response width ≤ 1.5 and 0.4 for F-region investigations
Transmitter Waveforms	Maximum duty cycle $\geq 10\%$ Maximum pulse width ≥ 1 ms Bandwidth ≥ 2 MHz
Assumed Sky Temperature, K	40
Receiver Bandwidth, MHz	20
Receiver Dynamic Range, dB	≥ 40
Receiver Output	At a convenient intermediate frequency

Table 1. Recommended HAARP ISR Performance Specifications, taken from:
"Final Report of the Alaskan Diagnostic Radar Panel", Co-Chairmen: William E. Gordon and Brenton J. Watkins, August 2000.

The radar approach is driven largely by the coverage and the beam motion requirements. A dish type antenna provides synoptic coverage, but the beam motion is restricted to a practical maximum of approximately 10° per second. A fixed phased array antenna is limited in synoptic coverage but can provide rapid beam pulse-to-pulse motion. A combined approach could provide broad synoptic coverage and rapid beam motions over a limited cone angle.

During the past several years, the National Science Foundation NSF has sponsored SRI International (SRII) to develop a 449 MHz modular, prototype phased array radar. HAARP is cooperating with NSF to test the SRII radar at the Air Force Research Laboratory Ipswich, MA radar range. During the summer of 2002, two 32-element panels were installed and demonstrated at the HAARP Site as shown in Figures 1 and 2.

Figure 1. NSF Sponsored, SRI International developed 449 MHz radar as installed and demonstrated at HAARP during Summer 2002.

During the next several years HAARP plans to develop a permanent infrastructure for incoherent scatter radar (ISR) and acquire a number of 32-element panels that would provide HAARP with a basic diagnostic radar that could be modularly expanded to a fully capable ISR. The permanent infrastructure will include a gravel pad on which such a radar would be installed, an access road, and provisions for commercial electric power, telephone, and networking for radar control and data acquisition. Figure 3 shows the layout of the ISR assess road and pad at the HAARP Research Station..
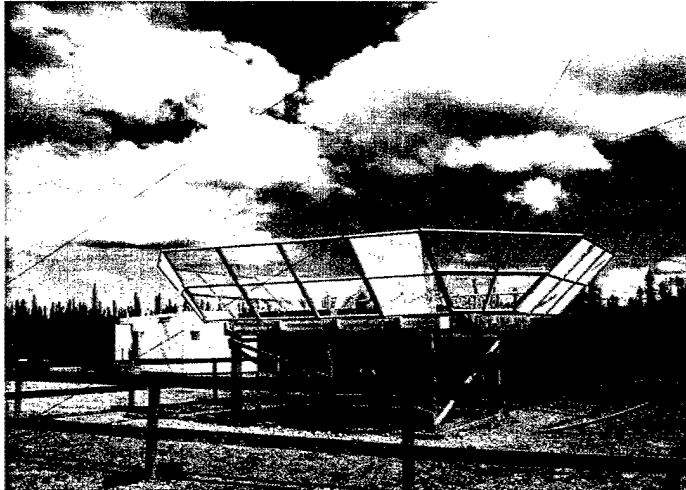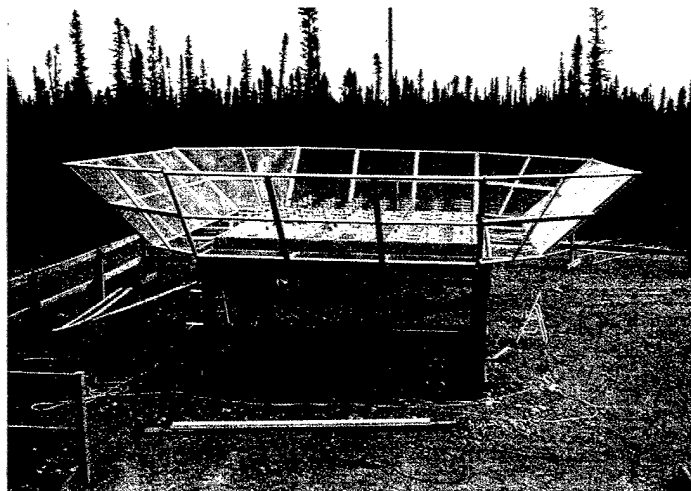

Figure 2. Looking down on the 64 element 449 MHz radar at HAARP with the installed clutter fence.
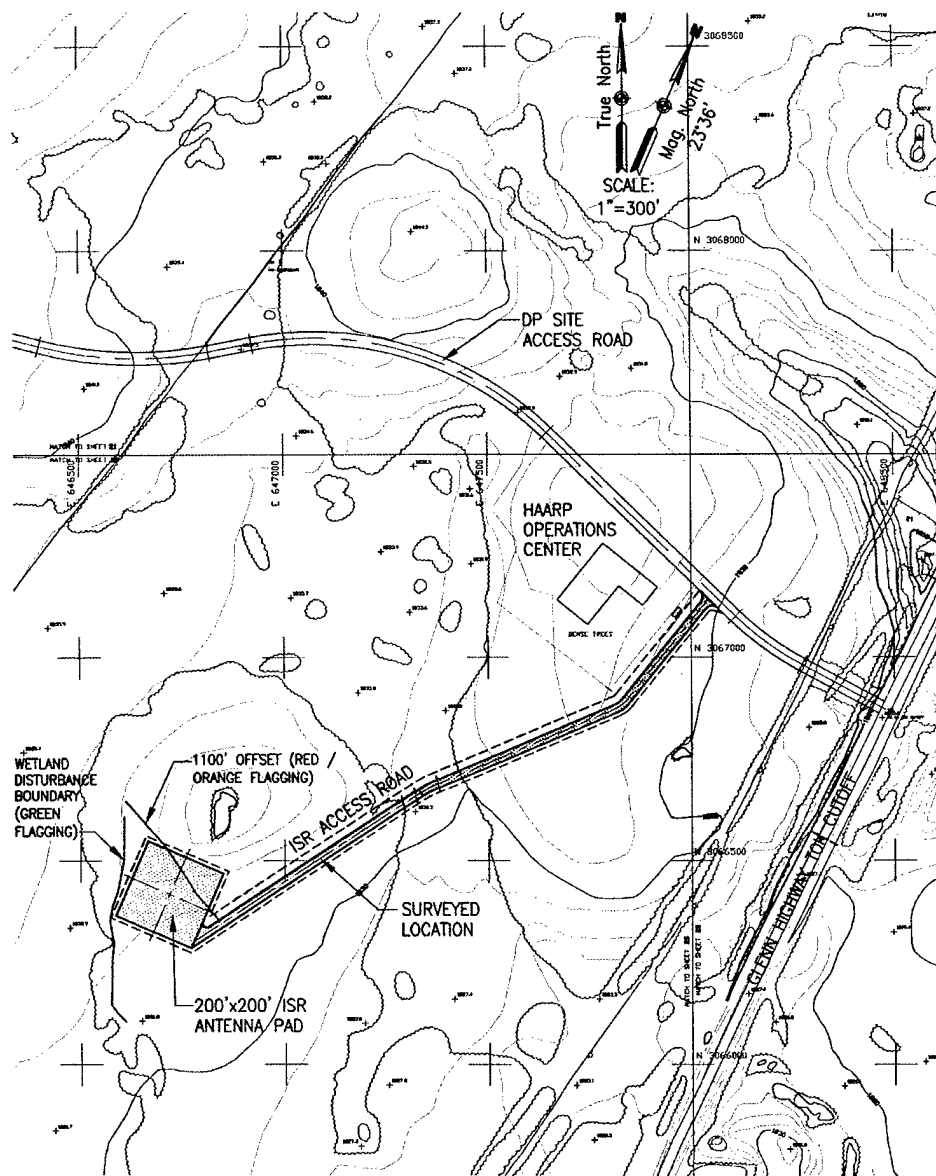
Figure 3. Planned permanent HAARP site location for an incoherent scatter radar showing the 200' square gravel pad and the access road. The array will be oriented magnetic North-South / East-West.

13. RF Spectrum Monitor
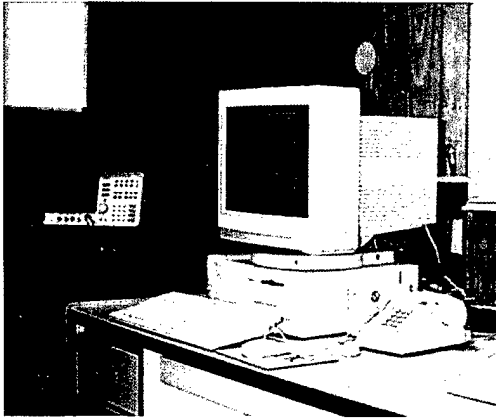
Edward J. Kennedy
Naval Research Laboratory

Introduction

Figure 1. The HAARP Spectrum Monitor and weather station.

The HAARP spectrum monitor is a continuously operating, automated system for recording and evaluating the electromagnetic environment at the HAARP facility to support the Electromagnetic Compatibility Program. Current and archived data are available over the Internet either through access to the HAARP FTP server or through the HAARP web site. All data are archived locally and remotely and can be obtained over the Internet in real time.

This diagnostic was operated temporarily during the summer of 1993 to obtain information about the spectral occupancy at the proposed HAARP and it has been in continuous operation since September 1994 to monitor all HAARP transmissions for spectral purity and compliance with various regulatory agreements. When not in use for this primary function, the system provides charts of propagation conditions in the High Frequency range.

Equipment Description

The Spectrum Monitor system is designed to operate in the high level RF environment near the HAARP HF Transmitter to monitor its spectral purity for compliance with regulatory requirements. It consists of a dual band antenna system, a high performance amplifier/filter front end, a high performance spectrum analyzer and a computer controller and data archiver.

Two separate antenna systems allow sampling of the background RF environment over the frequency range 1 MHz to 1 GHz. The HF antenna covers frequencies up to 30 MHz using two crossed dipoles, resonant at a frequency near the top of the HF band. A broadband coupling network and coaxial transmission line deliver received signals to an amplifier/filter module located in the operations center. The input stage is a high dynamic range, low noise amplifier that can be bypassed during HAARP heater operations to prevent saturation. Under these conditions, fixed attenuators can be switched into the amplification chain to preserve linearity.

Frequencies above 30 MHz are monitored using a broadband discone antenna mounted on the top of a 60-foot tower. A low loss coaxial line connects this antenna with the first stage of amplification located at the base of the tower. The amplifier front end is

protected with a high pass filter exhibiting steep attenuation for frequencies below 10 MHz (where the HAARP heater operates). This amplifier is followed by an additional high pass filter and further amplifier stages. The resulting frequency characteristic produces a low noise, highly linear system for all frequencies above 30 MHz. This portion of the system is extremely sensitive to unwanted transmitter products (such as harmonics and spurious signals) that could be produced by an equipment malfunction or mis-adjustment.

The conditioned signals are fed to an HP-8560 spectrum analyzer, which is controlled using the IEEE-488 standard instrument bus from a desktop computer. The computer runs continuously under reconfigurable scripting software and spectrum monitor data are archived either locally or on the HAARP networking computer. A weather station is also connected to the desktop computer and continuous information about the local weather conditions is also archived.

Products

The spectrum monitor system has produced a continuous sample of the background RF environment at the Gakona site since December 1994. The data is archived and includes operational periods as well as the quiescent background. Beginning in 1996, additional products were made available over HAARP website. These include running signal strength charts for various signals of opportunity (such as WWV) as received at the Gakona site and general HF band waterfall charts (see Figure 2) that provide general descriptions of the background HF propagation conditions. A real time spectrum monitor sweep, updated each 20 minutes, is made available on the HAARP website.
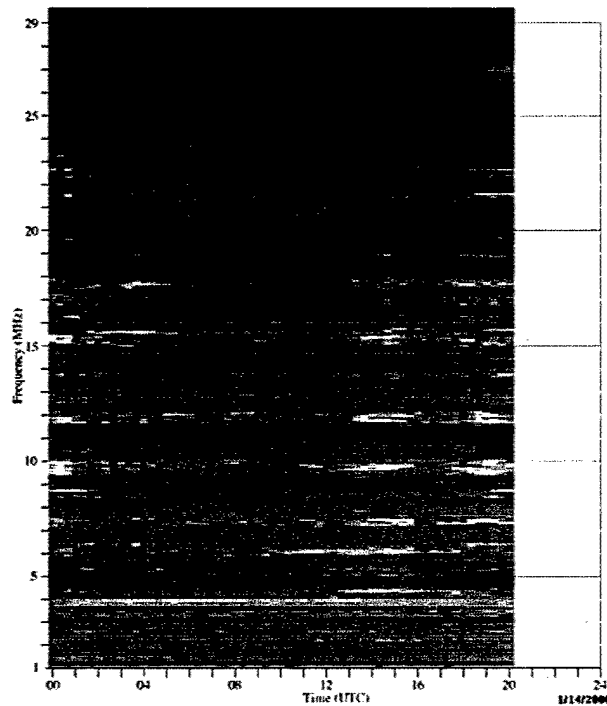

Figure 2. Spectrum Monitor waterfall chart covering the 2-30 MHz HF spectrum.

Programmability

Although the primary function of the spectrum monitor is to evaluate the performance of the high power HF transmitter system, the programmable controller may be used for research purposes where single frequency or swept frequency measurements are to be made. Sensitivity in the HF band is background noise limited at frequencies below approximately 20 MHz. In the VHF/UHF bands, the system performance is limited by the omnidirectional, low gain, probe antenna system.

68

14. Optical Telescope

U. S. Inan, E. A. Gerken
STAR Laboratory, Stanford University

Introduction

The goal of this experiment is to make telescopic measurements of the optical emissions created by HAARP HF heating of the ionosphere. With the narrow field of view (0.72° x 0.9°) of a telescopic system we will be able to determine whether there is fine structure in the optical airglow emissions. We are able to view an object 100 km away with a resolution of ~3m. Since the lateral extent of the ionospheric region heated by the HAARP HF transmitter is ~30 km, our narrow field of view is completely within the heated region.

Although airglow observations of heaters have been conducted in the past, our observations constitute the first attempt to look for fine structure within the heated regions. Observing either the absence or presence of structure would be an important scientific contribution and would give additional insight into the atmospheric makeup of these heated regions. Although the main lobe of the HAARP HF heater is quite broad, one might expect fine structure due to ambient electron density variations. It is also possible that small variations in radiation pattern within the main lobe may be detectable.

Instrumentation

The system consists of a telescope with a cooled, bare CCD camera mounted at the image plane of the telescope. The system uses a Meade Starfinder telescope which is a 16" aperture, f/4.5 Dobsonian-mounted, Newtonian reflecting telescope. The camera is narrowband-filtered to allow either the near infrared N2 first-positive lines, the 630nm oxygen line, or the hydroxyl lines to be selected for viewing. The camera is a
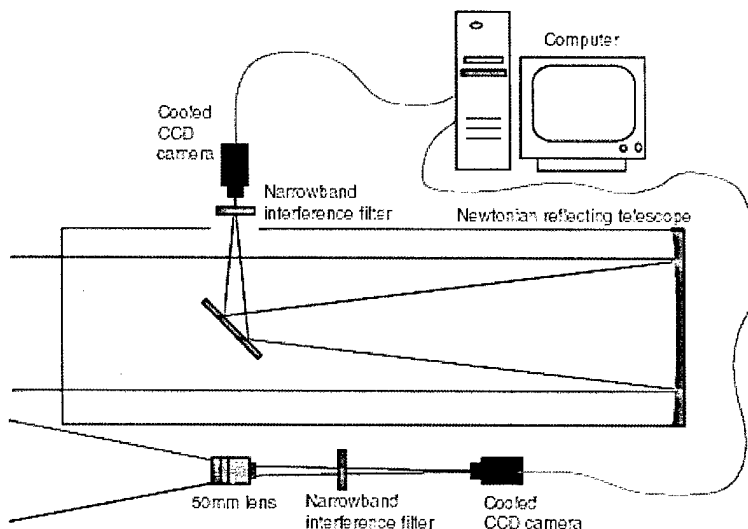

Figure 1. Optical Telescope.

Princeton Instruments VersArray 512B digital CCD system with thermoelectric Peltier cooling, 512 × 512 pixel format, and binning and subregion readout modes. Frames from the camera are sent directly to a computer interface with accompanying software for real-time acquisition, display, and data processing as shown in Figure 1. The interface has a 16 bit A/D converter with dual speeds of 100 kHz and 1 MHz. The camera is integrated for several seconds (up to 30sec) to be able to view the relatively dim airglow levels of 20-100 R.

Figure 2 shows data images that were acquired on Day 99 during the April 2000 HAARP campaign. The narrow field of view (0.72 x 0.9 degrees) image was taken using the telescope aimed at zenith. The wide field of view (9 x 12 degrees) image was taken using a bore-sighted camera. Both cameras were intensfied CCD's and were narrowband filtered at 630nm. Due to the 38 second exposure time, stars are observed as trails of light in the telescope whereas they are only pinpoints in the wide field of view. GPS time is stamped in the lower left corner of each image.
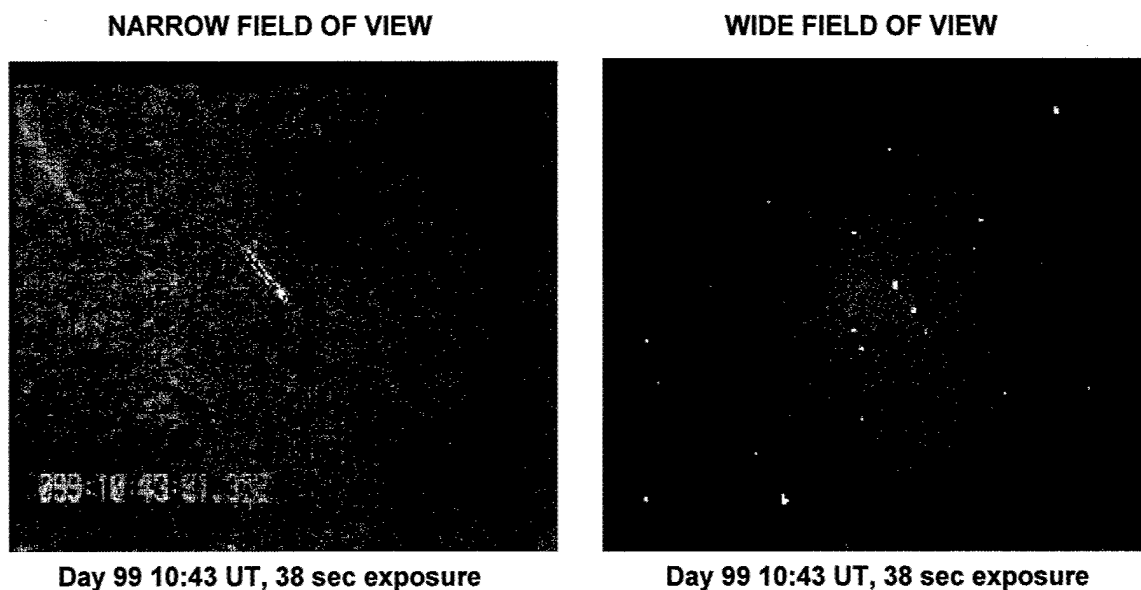
NARROW FIELD OF VIEW **WIDE FIELD OF VIEW**

Day 99 10:43 UT, 38 sec exposure   **Day 99 10:43 UT, 38 sec exposure**

Figure 2. Example of data from the April 2000 HAARP research campaign.

14. Optical Imager

Todd Pedersen, Air Force Research Laboratory
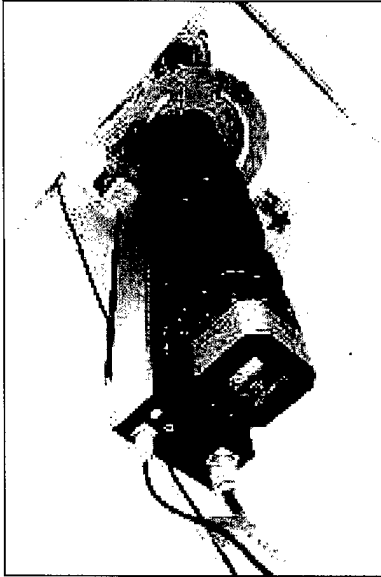Peter Ning, Scion Associates

Figure 1. The HAARP imager installed in the optics shelter.

The HAARP imager is a sensitive yet versatile imager designed specifically to observe the low-intensity optical emissions produced during ionospheric heating experiments. It also provides valuable diagnostics of the naturally occurring geophysical background including auroral particle precipitation and F-region plasma density structures. A variety of operating modes and accessories can be selected to customize the instrument for specialized measurements. Periodic laboratory and on-site calibrations of the imager allow raw data from standard operating modes to be accurately converted to relevant geophysical parameters. Because of the large number of permutations of instrument options and settings, calibrations for non-standard modes are not available unless arranged through the principal investigator.

Standard Configuration

In the default configuration, the imager is equipped with a 180° fish-eye lens and oriented vertically to observe the entire sky. Light from the all-sky lens then passes through one of up to five 3-1/2 inch diameter narrow-band (~2 nm) filters mounted in an automatically controlled filter wheel. After filtering, the image is focused on a cooled 25 mm Gen-2 inverter intensifier, which has 4 logarithmically spaced gain levels ranging up to a maximum of 90,000. The amplified image emerging from the other side of the intensifier is passed by relay optics to a cooled CCD camera containing a 512 x 512 pixel CCD chip. Electron counts in the CCD wells are summed in 4-pixel blocks to form a 256 × 256 pixel image, which is then digitized in mid-gain mode at 12-bit resolution and passed to a networked Linux PC through a custom buffer box attached to an EPP parallel port. Commands to the imager are carried through a serial port control interface. The Linux operating system allows full imager control and data monitoring from any location with internet access. The imager has been operating routinely in automated mode since September 1999.
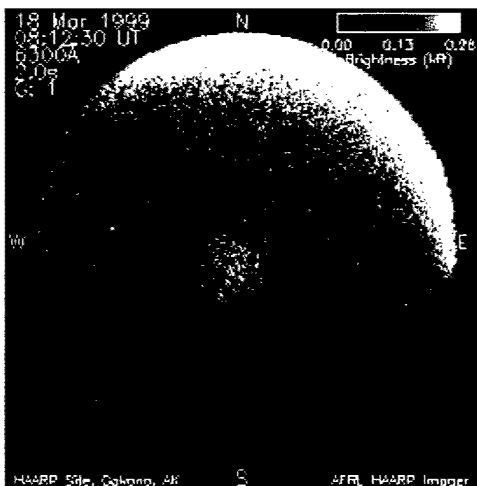
Figure 2. A red-line all-sky image showing the natural aurora at the top and heater-produced emissions at the center.

Options

The standard 180° all-sky lens can be manually replaced with a 16° narrow-field lens, increasing spatial resolution by a factor of ~10 at the expense of decreased sensitivity and field of view. Up to five filters can be used in an observing sequence, or a filter position can be left empty to capture white-light images. Filters not already in the wheel must be manually installed before the experiment. In addition to the 4 intensifier gain settings, the CCD camera has three gain ranges (LO, MID, and HI) providing a range of compromises between sensitivity, dynamic range, and read noise. CCD spatial resolution can also be switched between 256×256 pixels and 512×512 pixels. The former format sacrifices spatial resolution to provide 4 times the brightness sensitivity of the latter, at one-fourth the data file size (~130 kB for 256×256 pixel images). The current data acquisition software is set up to cycle once per minute through a user-programmed sequence of filter wheel settings and exposure times, which can be adjusted in steps of 1/10 sec from the minimum of 0.2 sec. For synchronization with other observations, the program allows each exposure to be started at a specified time within the minute, provided acquisition of the previous image is complete. Exposure times longer than 1 minute are possible but require modification of the standard software by the instrument PI. The data acquisition system was upgraded in the autumn of 1999 to include an automatic gain and exposure control option that uses statistical sampling of image data points to center the dynamic range on features of interest and prevent over and underexposures during automated operation. Under the automated gain control system, users may specify the sampling pattern, number of sample points, and desired standard deviation. . In addition to the default fixed vertical mount, the imager can also be mounted on a steerable platform for tracking and off-zenith observations. The platform can hold up to 300 lbs payload (including the ~100 lb imager), has 0.25° angular resolution, and 0-360° azimuth and 0-100° elevation travel. Processed data from the imager is now available through the HAARP web page in real time (http://maestro.haarp.alaska.edu/haarp/imager/latest.html). This includes false-color displays for each filter approximating the true color of the emission, annotation and overlays of image parameters such as date, time and exposure time, and a data scale giving approximate intensities in rayleighs (see Figure 3). Data from the imager will be available in NetCDF format in the near future.
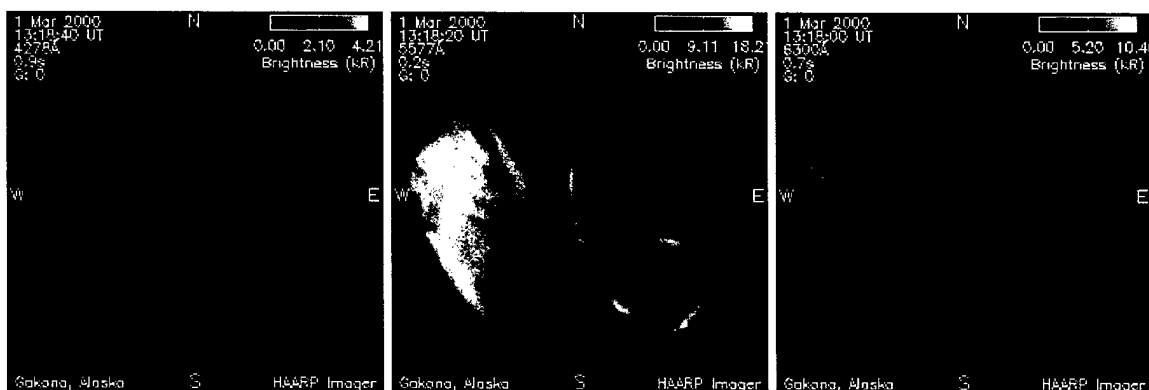
Figure 3. Example of annotated false color images available in real time through the HAARP web site.

Imager Feature	Method of Selection	Options and Specifications (* denotes default configuration)
Objective lens	Manual	*180° (resolution 0.36 deg/pixel in 512×512 format) 16° (resolution 0.03 deg/pixel in 512×512 format)
Filters	Programmable (up to 5); manual installation required for changes from default	*None (white light) *428.2 nm (21.9 Å width; max. sensitivity 4 R·sec) 486.7 nm (28.6 Å width; max. sensitivity 2.5 R·sec) 530.0 nm (24.7 Å width; max. sensitivity 2.5 R·sec) *558.1 nm (15.8 Å width; max. sensitivity 2.5 R·sec) *630.4 nm (15.6 Å width; max. sensitivity 4 R·sec) *777.8 nm (15.6 Å width; max. sensitivity 8 R·sec)
Intensifier	Programmable	4 gain levels stepped by factors of 2
CCD resolution	By Request Only	*256×256 pixels (4X sensitivity increase, 130 KB file size) 512×512 pixels (500 KB file size)
CCD Gain	By Request Only	LO (gain 91 e⁻/count; read noise 63 e⁻) *MID (gain 49 e⁻/count; read noise 39 e⁻) HI (gain 25 e⁻/count; read noise 24 e⁻)
Exposure time	Programmable	0.2->100 s in steps of 0.1 sec.
Cycle time	By Request Only	Default of 1 minute; software can be modified if necessary
Timing	Programmable	Shutter opens on user-specified second within minute. Possibility of data loss if sufficient time not allowed for exposure and data transfer. Clock synchronized to HAARP time server
Mount	Manual installation on stage; stage motion is programmable	*Fixed zenith pointing Programmable stage; 300 lbs max payload, 0.25° angular resolution, 0-360° azimuth & 0-100° elevation travel

73